Nanoscale

REVIEW

View Article Online
View Journal | View Issue

Cite this: *Nanoscale*, 2023, **15**, 4170

Two-dimensional nanomaterial MXenes for efficient gas separation: a review

Yuanyuan Wang, Zhenhua Niu, Yangyang Dai, Peng Mu* and Jian Li *

Transition metal carbides/nitrides (MXenes) are emerging two-dimensional (2D) materials that have been widely investigated in recent years. In general, these materials can be obtained from MAX phase ceramics after intercalation, etching, and exfoliation to obtain multilayer MXene nanosheet structures; moreover, they have abundant end-group functional groups on their surface. In recent years, the excellent high permeability, fine sieving ability and diverse processability of MXene series materials make the membranes prepared using them particularly suitable for membrane-based separation processes in the field of gas separation. 2D membranes enhance the diversity of the pristine membrane transport channels by regulating the gas transport channels through in-plane pores (intrinsic defects), in-plane slit-like pores, and planar to planar interlayer channels, endowing the membrane with the ability to effectively sieve gas energy efficiently. Herein, we review MXenes, a class of 2D nanomaterials, in terms of their unique structure, synthesis method, functionalization method, and the structure–property relationship of MXene-based gas separation membranes and list examples of MXene-based membranes used in the field of gas separation. By summarizing and analyzing the basic properties of MXenes and demonstrating their unique advantages compared to other 2D nanomaterials, we lay a foundation for the discussion of MXene-based membranes with outstanding carbon dioxide (CO_2) capture performance and outline and exemplify the excellent separation performances of MXene-based gas separation membranes. Finally, the challenges associated with MXenes are briefly discussed and an outlook on the promising future of MXene-based membranes is presented. It is expected that this review will provide new insights and important guidance for future research on MXene materials in the field of gas separation.

Received 27th November 2022,
Accepted 27th January 2023

DOI: 10.1039/d2nr06625d

rsc.li/nanoscale

1 Introduction

With the occurrence of global warming, the level of carbon dioxide (CO_2) in the atmosphere has increased dramatically. Consequently, this has accelerated a variety of global environmental and biological problems, including the greenhouse effect, ecosystem disruption, ocean acidification and recognized climate-induced species extinction.[1–7] Therefore, environmental awareness has gained significant interest worldwide, prompting the scientific community to find ways to deal with climate change. In this case, achieving the "double carbon goal" has become the focus of major strategic decisions in China, and it is urgent to address the huge impact of the increasing CO_2 content in the atmosphere on climate change. Currently, the commonly used CO_2 capture methods include charge modulation,[8] coupled electrochemical CO_2 conversion,[9] steam regeneration,[10] solvent absorption,[11] photocatalysis,[2,12] and membrane-based capture (membrane separation).[13,14] However, some of these methods have shortcomings such as secondary pollution, low efficiency, high energy consumption, high cost, and complicated operation and maintenance, which greatly limit their large-scale practical application.[15–17] Among them, membrane separation is an indispensable gas purification technology that can effectively reduce the carbon footprint, which is not only a large-scale comprehensive energy-saving technology but also one of the most effective ways to capture CO_2.[18,19] Thus, it has been applied in many fields such as organic dye adsorption, seawater desalination, and osmotic evaporation.[20–23] In the field of gas separation, membranes can purify mixtures through selective interactions with target molecules and the synergistic construction of multiple separation mechanisms, thus opening up new avenues for the industrial separation of CO_2.[24–26] In the past few decades, the membrane separation technology has been recognized as an attractive and environmentally friendly carbon capture technology due to its low cost (capital and operational), ease of operation, high separation efficiency, energy efficiency, and environmental friendliness. Its role in solving energy and environmental challenges in modern industry and daily life is

Key Laboratory of Eco-functional Polymer Materials of the Ministry of Education, College of Chemistry and Chemical Engineering, Northwest Normal University, Lanzhou 730070, P. R. China. E-mail: pengmu2019@nwnu.edu.cn, jianli83@126.com; Tel: +86 9317970806

important.[27,28] Membrane materials with good selectivity and high permeability are the key to achieving efficient membrane separation.[29,30]

At present, several solid-state materials are widely used in the field of gas separation, which exhibit a good performance, as shown in Table 1.

In addition to these common materials, with the development of scientific research, other types of materials are also used in the field of gas separation, such as 2D transition metal sulfides (TMDs).[46] In summary, 2D materials with nanoscale thickness play an important role in membrane separation technology. In nanomaterial science, 2D nanostructures are very attractive for the fabrication of nanodevices due to their high surface-to-volume ratio and good compatibility with device design.[47] Moreover, 2D materials enable the development of high-performance separation membranes due to their planar laminar flow structure, high spreading chord ratio and tunable surface features. Thus, they are important materials for advanced molecular separation. The extraordinary permeability of membranes prepared using these 2D materials opens up new avenues for the ultra-fast and highly selective separation of water and gases. Consequently, an increasing number of researchers have devoted their efforts to synthesizing and functionalizing 2D nanosheets in a controlled manner to obtain materials with enhanced performance.[48–55]

Interestingly, a new group of highly promising 2D materials, called transition metal carbides and nitrides (MXenes), have attracted interest from many researchers in the last few years due to their easy-to-produce 2D structure, tunable surface chemistry and interlayer spacing. $Ti_3C_2T_x$ was first reported in 2011, and in the decade since, it has been increasingly widely used in various synthesis procedures and applications.[56–59] As a new type of 2D ceramic nanosheet, MXenes are being investigated and widely applied in the fields of sensors, electrochemistry, medicine, biology, energy and electronics.[60–63] Simultaneously, they have also been investigated for practical applications in various research fields, such as lubricants, photodetectors, solar cells, energy harvesting and storage, as shown in Fig. 1.[64–71] Presently, MXenes are considered as molecular barriers with ultra-thin atoms because of their several atomic-thick layers. Consequently, they can be employed for the synthesis of outstanding high-performance barrier separation membranes, thus showing promise for realizing higher permeability properties.[72,73] The unique properties of MXenes lead to new applications compared to other

Fig. 1 Some of the application areas of MXenes.

Table 1 Solid materials with a wide range of applications and good performances

Material	Advantage	Prospect	Application	Ref.
Graphene	Single atoms and can be prepared as high permeability and thin membrane	Synthesis of high flux selective gas separation membranes	Ion-gated graphene film	31 and 32
GO	Hydrophilic 2D crystalline nanostructures contains oxygen functional groups	Capable of efficient CO_2 separation	SDBS-modified GO membrane for gas purification technology	33 and 34
g-C_3N_4	2D layered material, capable of synthesizing ultra-thin layered nanochannels with selective loading of different active ions	Preparation of high selectivity separation membranes	A novel SILM was constructed by IL through nano-constrained [EMIm][AcO] in the 2D channel of g-C_3N_4	35–37
BNs	High specific surface area, abundant structural defects, low density and excellent chemical inertness	Preparation of high permeability separation membranes	A novel BN nanosheet-supported magnetic ionic liquid membrane (BN-SMILM) was constructed by confining nano MIL $[P_{6,6,6,14}][FeCl_4]$ to 2D nanochannels	38–40
MOFs	Ligand compounds with tunable, designable and functionalizable nanospaces	Preparation of high permeability and high selectivity separation membranes	Design and preparation of novel MOF-based hybrid films on tubular ceramic substrates to form thin and compact MOF/silicone nanocomposite films	41–43
COFs	An emerging class of porous crystalline materials with tailored functionality and carefully designed stable and ordered frameworks	Achieving efficient CO_2 capture to mitigate the greenhouse effect	Most likely a viable alternative to MOF, thus meeting the multifaceted requirements for activation and conversion of CO_2	44 and 45
...	...	...	...	...

2D membrane nanomaterials, such as graphene and zeolites. Generally, three strategies are employed for the preparation of MXene-based membranes: (1) MXenes are used as skeleton materials to directly prepare 2D membranes with a layered structure; (2) different polymers or nanomaterials are combined with MXenes to prepare composite membranes; and (3) MXenes are used as coating materials to modify the original support layer to prepare membranes. The MXene composite films prepared using the above-mentioned methods possess randomly stacked adjacent nanosheets, forming disordered interlayer "nanochannels" for mass transport between them. The interlayer stacking enables the passage of molecules, thus achieving the selective separation of large molecular compounds, while also allowing small molecules to move between the channels, which is a process known as "molecular sieving".[74–76] MXenes have high energy saving separation performance due to their structure and special chemical surfaces, and their modifiable property allow the prepared membranes to exhibit superior performances in a variety of separation sciences. This has created numerous opportunities for researchers to fabricate novel materials, such as energy-efficient membranes for various engineered separations.[77] In recent years, the excellent chemical, mechanical, optical and separation properties such as remarkable flexibility, hydrophilic surface, high mechanical strength and good electrical conductivity of the MXene series materials have made them suitable for a wide range of membrane-based separation processes.[78–84] Their applications include gas separation, pervaporation, desalination and solvent/water separation.[85–88] Nonetheless, the application of MXenes in gas separation membranes is still in its infancy.

Herein, we review the research related to 2D MXene nanomaterials and the separation membranes prepared using them. Firstly, the basic structure, synthesis and functionalization of MXenes are briefly introduced (section 2). Then, the properties of MXene-based films are summarized and reviewed, as well as the structure–property relationship (effect of structure on performance) of MXenes in their design and fabrication (section 3). Finally, a comprehensive summary of MXenes is presented, including the gas separation performance of various MXene membranes, their advantages and disadvantages in the field of gas separation, the remaining challenges that need to be urgently addressed, and the future prospect of this discipline (section 4).

2 Basic structures of MXenes and methods for their synthesis and functionalization

In recent years, 2D MXene materials, represented by $Ti_3C_2T_x$ prepared by etching Ti_3AlC_2 (MAX phase), have attracted great attention in the energy and environmental fields because of their large layer spacing, good environmental flexibility and large specific surface area.[89,90] MXenes not only have 2D nanostructures with high aspect ratio, but also diverse surface end groups, which offer the possibility of functionalization.

2.1 The basic structure of MXenes

MXenes are transition metal carbides and carbonitrides or nitrides with a layered structure obtained by the selective etching of MAX phase precursors, which are expressed by the formula $M_{n+1}AX_n$ (n = 1, 2, and 3) (where M represents early d-block transition metal, A is the main group element (mainly IIIA or IVA), and X is C and/or N).[91–93] As shown in Fig. 2a, the original MAX phase (Fig. 2d) was prepared by a series of processes including etching and layering exfoliation to finally obtain MXenes for storage. Atomic force microscopy (AFM) measurements showed that the synthesized MXenes had a thickness of single flakes of around 1.5 nm, and the lateral dimensions of the MXene flakes during their synthesis varied from nanometers to micrometers (Fig. 2b). During the typical synthesis of MXenes, the MXene stacks (Ti_3C_2 or Ti_2C) are allowed to adhere to each other by etching the MAX precursors (*i.e.*, Ti_3AlC_2 or Ti_2AlC) in an etching solution (HF or acidic fluoride) at ambient temperature. This process selectively removes the Al(A) species and terminates the carbide layer surface by –OH, –F and –O– groups (Fig. 2c and g). The scanning electron microscopy (SEM) and transmission electron microscopy (TEM) images also showed that after etching, the multilayer accordion-like MXenes were stacked together by van der Waals forces and hydrogen bonding, and the exfoliated MXene nanoflakes were relatively thin. It showed the basal hexagonal structure and the absence of obvious nanoscale defects and carbide amorphization in the MXene flakes (Fig. 2e and f).[75,94–97]

2.2 Method for the synthesis of MXenes

MXenes, due to their adjustable structure and rich surface chemistry, have become a versatile material. As a promising 2D material, the physical and chemical diversity of MXenes endow them a wide range of applications.[98] With the development of methods for the large-scale preparation of MXene nanosheets and derivatives, a variety of synthetic routes has been proposed.[56] Synthesis routes with high efficiency lays the foundation for broadening the application scope of MXene materials. Since MXenes were first reported in 2011, their synthesis has been rigorously investigated by the scientific community, including the use of a variety of different physical and chemical routes. At present, various synthesis strategies have been developed to etch the MAX phase to achieve rich terminal groups and unique properties.[99,100] The MAX phase is a three-dimensional (3D) structure before being etched, and through a certain etching process, it can be transformed into MXenes with a 2D lamellar structure.[94] As shown in Fig. 3, the etching method and layering strategy for the synthesis of MXenes are included. In general, MXenes are synthesized *via* the top-down etching process with the layered ternary MAX phase as the precursor, and the "A" layer is selectively etched from the MAX phase with an appropriate etchant.[101] The MAX phase will break the chemical bond between the M and A elements

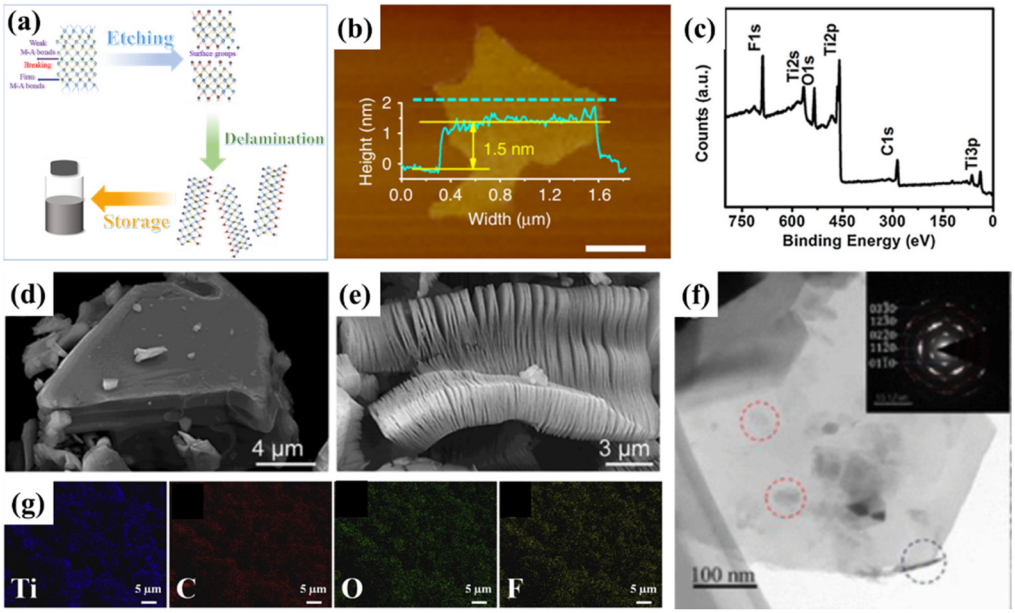

Fig. 2 (a) MXene preparation process. (b) AFM of $Ti_3C_2T_x$ MXene flakes. Reprinted with permission.[75] Copyright 2018, Springer Nature. (c) XPS survey of $Ti_3C_2T_x$ MXene. Reprinted with permission.[97] Copyright 2018, Elsevier. (d) SEM of $Ti_3C_2T_x$ MAX phase. (e) SEM of multilayer $Ti_3C_2T_x$ MXene. Reprinted with permission.[94] Copyright 2012, the American Chemical Society. (f) TEM of $Ti_3C_2T_x$ MXene flakes. Reprinted with permission.[95] Copyright 2016, the American Chemical Society. (g) EDX of $Ti_3C_2T_x$ MXene. Reprinted with permission.[96] Copyright 2018, Elsevier.

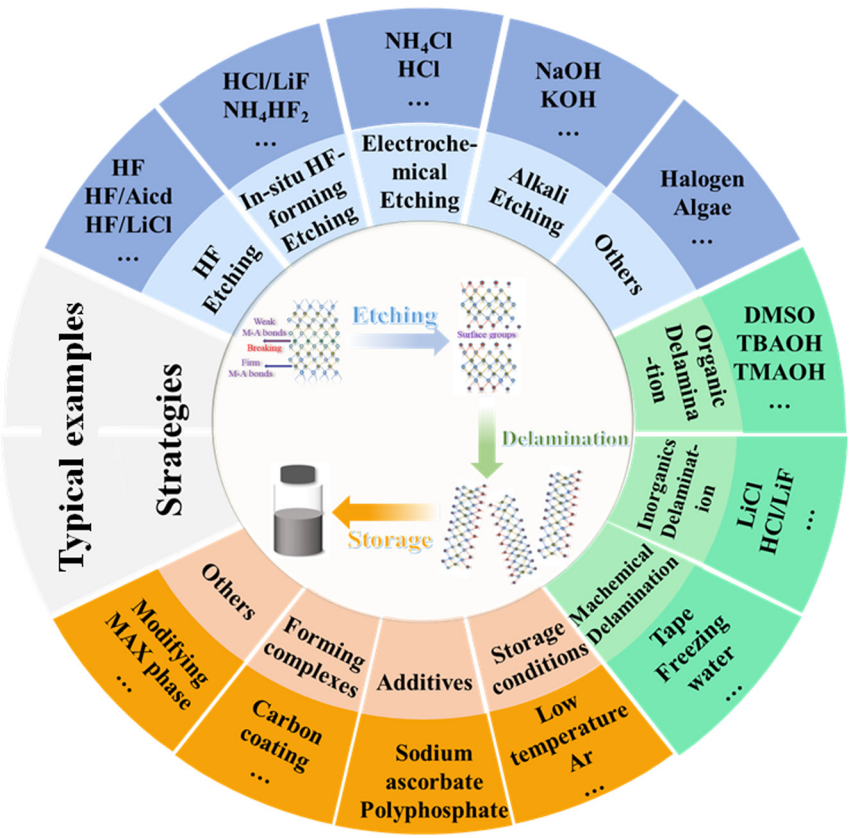

Fig. 3 Currently reported etching methods and layering strategies for the synthesis of MXenes.

during the etching process, and then the A elements are etched away. The M–X bond is stronger and has the characteristics of covalent/metal/ionic bond hybridization, while the M–A bond is essentially a metallic bond.[102] Under high-temperature conditions, both the M–A and M–X bonds are broken, forming a rock-like 3D structure.[89] Moreover, when etching with a strong corrosive etchant, both M and A elements are etched away and carbide derivatives are formed. Consequently, both etching methods should be used selectively to etch the A elements to obtain the target MXenes. Presently, dozens of MXenes with different configurations have been successfully synthesized. Understanding the different effects of using different etching methods and etchants on the structural characteristics and defects of MXenes is crucial in improving the performance of MXenes, optimizing the etching schemes and further exploring new MXene compositions. Also, the MAX phase is an important precursor for obtaining MXenes in high efficiency and high yield. Consequently, a variety of etching solutions has been used as etchants to date, including aqueous hydrofluoric acid (HF),[90,103,104] ammonium hydrogen fluoride (NH_4HF_2) is dissolved in water,[90,105–107] and lithium fluoride (LiF)/hydrochloric acid (HCl) mixtures.[103,108–112] Different etching conditions will lead to different MXene sheet sizes, synthetic yields, and surface-terminated functional groups, and these characteristics will also affect the physical properties and the chemical properties of the final synthesized MXenes.[72] Considering the diversity of MXene synthesis strategies, several commonly used MXene preparation methods are introduced here, including direct hydrofluoric acid (HF) etching and *in situ* HF etching.

2.2.1 The direct HF etching method. When HF etching is used, almost all the Ti_3AlC_2 particles can be etched to become $Ti_3C_2T_x$ in sufficient time because the etching of the precursor crystals will break the particles into smaller crystals along the grain boundaries.[90] HF is the first reported etchant to obtain MXene from its corresponding MAX precursor. In 2011, Gogotsi and Barsoum *et al.* found that the Al atomic layer in Ti_3AlC_2 can be selectively etched in 50% HF to obtain accordion-like $Ti_3C_2T_x$ under interlayer van der Waals forces and surface hydrogen bonding. This is due to the presence of Al in the MAX phase, which is highly reactive with –F. The etching mechanism of this process is shown in Fig. 4a.[113] It is noteworthy that the MXenes obtained using this etching process possessed abundant surface end groups such as –F, –OH and –O. The etching process can be defined as eqn (1)–(4), as follows:[114]

$$Ti_3AlC_2 + 3HF = AlF_3 + \frac{3}{2}H_2 + Ti_3C_2 \quad (1)$$

$$Ti_3C_2 + 2HF = Ti_3C_2(F)_2 \quad (2)$$

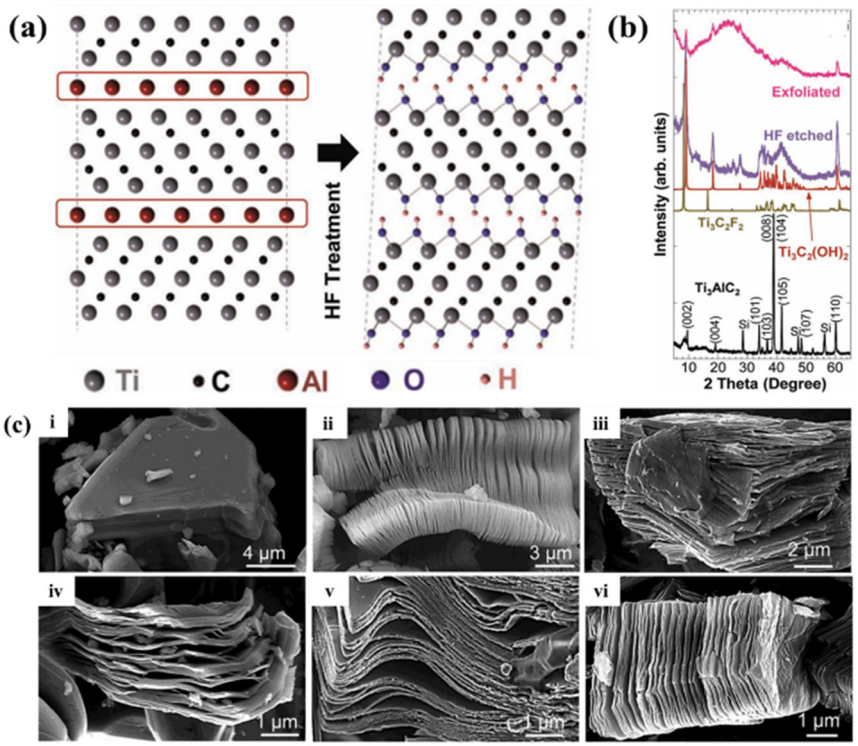

Fig. 4 Principle and product characterization by HF etching. (a) Schematic diagram of the exfoliation process of Ti_3AlC_2, showing the substitution of Al atoms by –OH after reaction with HF. (b) XRD images of Ti_3AlC_2 and ultrasonically exfoliated nanosheets before and after HF treatment. Reprinted with permission.[113] Copyright 2011, John Wiley and Sons. (c) SEM images of: (i) Ti_3AlC_2 particles, which are typical of the unreacted MAX phase, (ii) $Ti_3C_2T_x$, (iii) Ti_2CT_x, (iv) $Ta_4C_3T_x$, (v) $TiNbCT_x$, and (vi) Ti_3CNT_x. Reprinted with permission.[94] Copyright 2012, the American Chemical Society.

$$Ti_3C_2 + 2H_2O = Ti_3C_2(OH)_2 + H_2 \quad (3)$$

$$Ti_3C_2 + 2H_2O = Ti_3C_2(O_2) + 2H_2 \quad (4)$$

Fig. 4b shows the XRD spectrum of MAX during etching. It can be clearly seen that after reacting with HF, the characteristic peak of Ti_3AlC_2 at about 39° disappeared, and the (002) peak also shifted to a smaller angle. It can be calculated from the following Bragg eqn (5) that the etching process increased the original interlayer spacing of Ti_3AlC_2.[115]

$$n\lambda = 2d \sin\theta \quad (5)$$

where d (nm) is the layer spacing; n is the number of diffraction levels (n = 1); λ is the diffraction wavelength of X-rays; and θ is the diffraction half-angle. Fig. 4c shows the Ti_3AlC_2 MAX phase and MAX derivatives such as $Ti_3C_2T_x$, Ti_2CT_x, $Ta_4C_3T_x$, $TiNbCT_x$ and Ti_3CNT_x.[94] It can be seen from this figure that although these products are different, they all presented an accordion-like multilayer structure, which indicates that HF etching is universal for the preparation of MAX phase containing Al.

In the etching process, the HF concentration, etching temperature and etching time have important effects on the etching degree and morphology of products. Alhabeb *et al.* studied the etching of Ti_3AlC_2 at room temperature (RT) using HF etchants with different concentrations and different etching times (*e.g.*, 5 wt% 24 h, 10 wt% 18 h, and 30 wt% 5 h). The results showed that the etching time of MAX was shortened and the etching efficiency was improved under the condition of high HF concentration. The morphology of the 5 wt% HF-etched product, as shown in Fig. 5a, was almost the same as that of the Ti_3AlC_2 precursor. The XRD image, as shown in Fig. 5b, shows the formation of $Ti_3C_2T_x$, which indicated that the formation of the accordion morphology was not a sign of the successful etching of MAX to obtain MXene.[90] Although the morphology of $Ti_3C_2T_x$ etched with HF at different concentrations was obviously different, the characteristic (002) peak of the product was also located at 9.0°, and the interlayer spacing was 9.7 Å, reflecting that there was no relationship between the fluffiness of the accordion-like structure and the interlayer spacing of the MXenes. Additionally, given that the surface end groups of $Ti_3C_2T_x$ were formed during the etching process, the concentration of HF had a great influence on the type and content of surface end groups.[116] As shown in Fig. 5c, the characteristic (00l) peak of Ti_3AlC_2 gradually disappeared when the etching time was extended and the etching temperature was increased. Ti_3AlC_2 was etched in 50 wt% HF for 2 h, and the characteristic peak at around 39° completely disappeared when the temperature reached 50 °C. To obtain the same result, complete etching of Ti_3AlC_2 was achieved by simply extending the etching time to 15 h at room temperature. In addition, the (002) peak of the prepared $Ti_3C_2T_x$ shifted to a lower angle with an increase in the etching time, indicating that the interlayer spacing gradually increased.[104] Hence, when using this

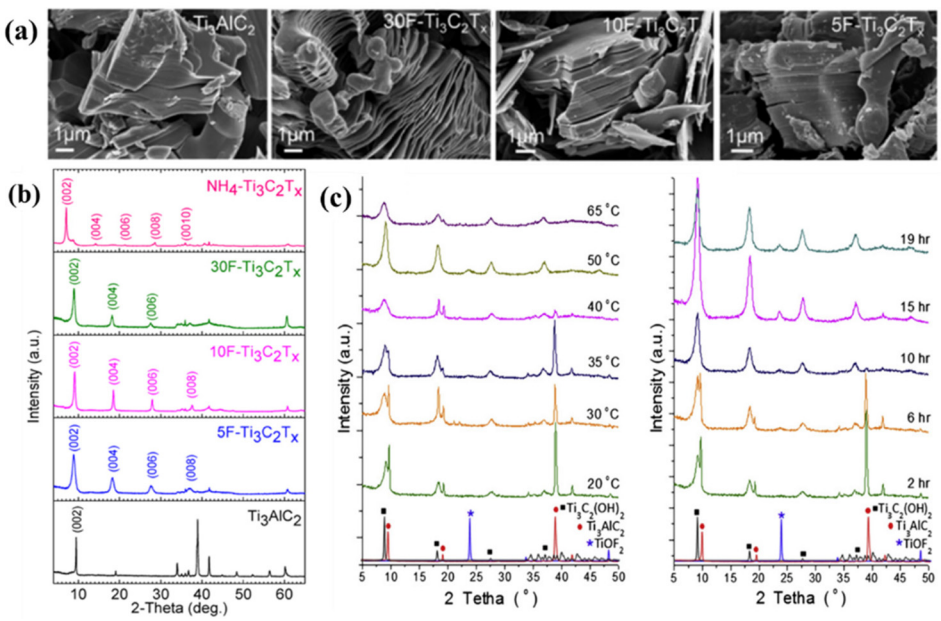

Fig. 5 Influence of different synthesis parameters on MXenes studied using the HF etching method. (a) Scanning electron microscopy images of Ti_3AlC_2 (MAX) powder, showing dense layered structures and multilayer $Ti_3C_2T_x$ powder synthesized from 5, 10 and 30 wt% HF. (b) XRD spectra of $Ti_3C_2T_x$ MXene powder and Ti_3AlC_2 powder synthesized from 5, 10 and 30 wt% HF etchants. Reprinted with permission.[90] Copyright 2017, the American Chemical Society. (c) Diffractograms were obtained after etching the Ti_3AlC_2 powder using 50% HF solution, with diffractograms at different temperatures on the left and diffractograms at different times at room temperature on the right. Reprinted with permission.[104] Copyright 2013, Elsevier.

method to synthesize MXenes, an appropriate HF concentration, etching time, temperature and other conditions should be selected according to different product requirements to better achieve the desired goal.

The HF etching method is simple, performed at low reaction temperature, and suitable for etching the MAX phase containing Al and some non-MAX phases. Nevertheless, HF etchants are an issue because of their high corrosion, toxicity, operational risks and adverse environmental impact. Moreover, the surface of the etched product has a large number of –F groups, which are not favorable for energy storage.[117,118]

2.2.2 *In situ* HF etching methods. To solve the corrosion problem of direct HF etching, it is necessary to explore and develop mild, non-toxic and environmentally friendly etching methods. Currently, fluoride salt mixed with acid etching has become a mature MAX phase etching method. This method involves the formation of HF *in situ* and the reaction between –F and the MAX phase containing Al due to the high reactivity of –F with the Al atom of the MAX precursor to form fluorine, H_2 and target MXenes. Employing different types of fluoride salts, the interlayer spacing of MXenes can be adjusted to meet the expected application requirements. With the development of research, other fluoride salts besides LiF have been used as etchants. Liu *et al.* mixed hydrochloric acid (HCl) with various fluoride salts (*i.e.*, LiF, NaF, KF, and NH_4F) to form a mixed solution for etching Ti_3AlC_2.[119] The reactions of both fluorinated salts and hydrochloric acid to form HF *in situ* can be described by eqn (6), as follows:

$$LiF(aq) + HCl(aq) = HF(aq) + LiCl(aq) \quad (6)$$

Due to the fact that the *in situ* HF etching process avoids the direct use of HF, this method has the advantages of simple operation, energy saving, and avoiding certain chemical risks during the etching process.

Acid/fluoride salt etching is the most common method for *in situ* HF etching, which refers to the selective etching of $Ti_3C_2T_x$ on the MAX (Ti_3AlC_2) phase with hydrochloric acid and fluoride salt.[103,107] When HCl/LiF is used as the etchant, the Li^+ ions can be spontaneously embedded between MXene layers. The intercalation of the metal ions increases the layer spacing between the MXene sheets, thus weakening the interaction between them, which eventually leads to the delamination of the MXene sheets during the washing process after they are etched.[90] In 2014, Ghidiu *et al.* first reported that HF was formed *in situ* with HCl/LiF solution at 40 °C for etching Ti_3AlC_2.[120] This method had successfully produced $Ti_3C_2T_x$ conductive clay with strong plasticity, which could be processed into films by rolling (Fig. 6a). The rollable MXene clay exhibited excellent elasticity, ultra-high toughness and good hydrophilicity, and it could be easily bent into an "M" shape

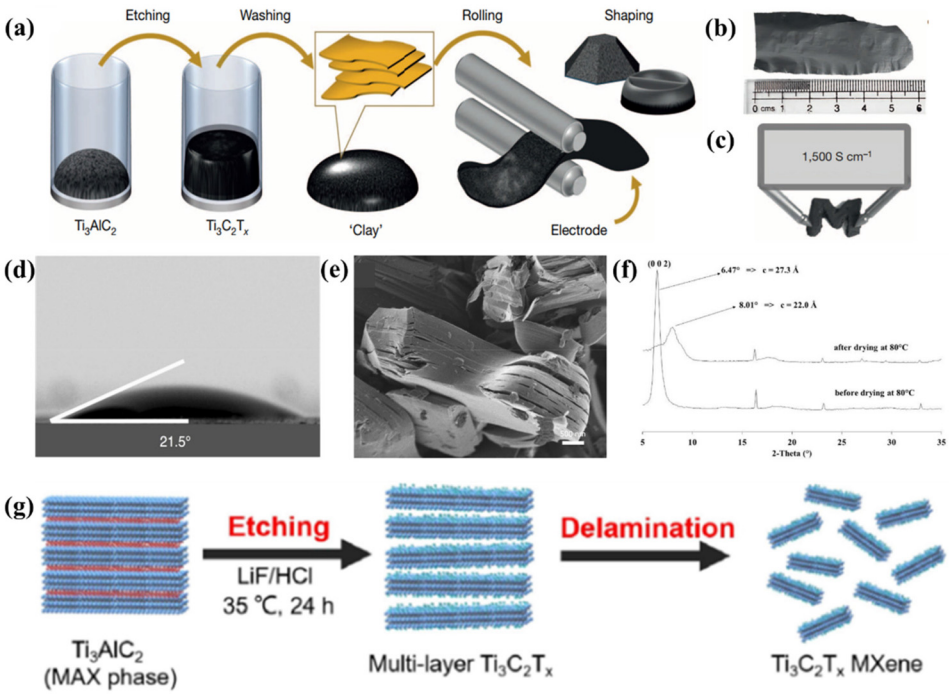

Fig. 6 Typical morphology and properties of Ti_3AlC_2 etched by HCl/LiF mixture etchant. (a) MAX phase is etched in a solution of acid and fluorine salts and washed with water to bring the pH to neutral, obtaining a clay-like deposit that produces a conductive object of the desired shape after the operation. (b) Digital photograph showing the morphology of rolled $Ti_3C_2T_x$ "clay" films. (c) Electrical conductivity of $Ti_3C_2T_x$ "clay" films. (d) Contact angle measurement of $Ti_3C_2T_x$ "clay" films. (e) Multi-layer MXene particles. Reprinted with permission.[120] Copyright 2014, Springer Nature. (f) XRD patterns of Ti_3C_2 before and after drying at 80 °C. Reprinted with permission.[121] Copyright 2013, The Royal Society of Chemistry. (g) Schematic diagram of the synthesis of $Ti_3C_2T_x$ MXene nanosheets. Reprinted with permission.[124] Copyright 2022, Elsevier.

and the electrical conductivity could be sustained up to 1500 S cm^{-1} (Fig. 6b–d). Similar to the process of direct HF etching, the process of forming HF etchant *in situ* with HCl/LiF for the synthesis of MXenes not only produced a multi-layer accordion-like morphology (Fig. 6e), but also enabled the surface of MXenes to be functionalized to produce rich surface terminal groups, such as –F, –OH, and –O. However, given that the latter reacts with acid and salt solution to produce HF, the obtained MXenes were inevitably accompanied by the insertion of water molecules, which led to a longer drying time for the product. The interlayer spacing of the MXenes obtained by *in situ* HF-forming etching was significantly reduced after drying due to the disappearance of water molecules inserted between the layers during the etching process (Fig. 6f).[121,122] The type of surface end base has a great effect on the interlayer spacing. This is due to the strong hydrophobicity of –F, which repels water molecules, making the interlayer spacing of MXene negatively correlated with the number of –F. Specifically, when the content of –F group increases, the interlayer spacing of the MXene will decrease. Zhu *et al.* also used the LiF/HCl etching method to prepare MXenes, as shown in Fig. 6g.[123] Briefly, 1.6 g of LiF was mixed with 20 mL of 9 M HCl. Subsequently, 1 g of Ti_3AlC_2 powder was added to the mixture and stirred continuously at 35 °C in a Teflon bottle for 24 h. After the etching process, it was washed repeatedly with deionized water to pH = 4–6. Finally, the product was sonicated under flowing inert gas conditions to obtain a layered $Ti_3C_2T_x$ MXene suspension. In this work, given that LiF was relatively mild, it reacted with HCl to produce HF *in situ*. Thus, the danger associated with the direct addition of HF was avoided and the safety of the experiment improved.

HF is not only volatile, but also dangerous to use. However, it can be replaced by the relatively mild NH_4HF_2. For the method of etching with NH_4HF_2 solution, Kim *et al.* first added Ti_3AlC_2 powder to an NH_4HF_2 solution and stirred it at room temperature for 24 h, and then washed the product to obtain etched MXenes.[125] In 2014, Barsoum *et al.* reported the fabrication of Ti_3C_2 films by selectively etching Al in epitaxial Ti_3AlC_2 films deposited by sputtering using NH_4HF_2 as the etchant.[105] The etching mechanism of this process can be summarized as eqn (7) and (8), as follows:

$$Ti_3AlC_2 + 3NH_4HF_2 = (NH_4)_3AlF_6 + Ti_3C_2 + \frac{3}{2}H_2 \quad (7)$$

$$Ti_3C_2 + aNH_4HF_2 + bH_2O = (NH_3)_c(NH_4)_dTi_3C_2(OH)_xF_y \quad (8)$$

Given that fluoride salts are solid at high temperatures, they have a higher level of safety during operation compared to hydrogen fluoride. However, to date, this above-mentioned method has only been proposed for etching Ti_3AlC_2 and has not been explored for other MAX phases.

Feng *et al.* used NH_4HF_2 as the etchant and obtained an MXene with a large interlayer spacing. When Ti_3C_2 was used as the electrode, the large layer spacing provided more space for ions to be embedded to store ions.[126] In this work, high-purity Ti_3C_2 MXene was prepared *via* a simple method, and the acquired Ti_3C_2 had a large layer spacing. Similar to the use of fluoride salts, NH_4^+ could increase the interlayer spacing by inserting MXene nanosheets.[127] The Ti_3C_2 etched by NH_4HF_2 in this work exhibited an outstanding pseudocapacitance performance, which was 34% higher than that etched by HF. Thus, NH_4HF_2 etching can produce Ti_3C_2 electrodes with excellent regeneration performance, which provides an effective way to improve the desalination performance of capacitive deionization technology.

In addition to the above-mentioned two *in situ* HF etching methods, there are other methods with similar principles for etching MAX phases. For example, Wu *et al.* reported a new mixed etchant, namely, NH_4F mixed with a low eutectic mixed solvent of choline chloride and oxalic acid, and then etched the MAX phase at different temperatures for 24 h *via* the hydrothermal process.[128] In this process, oxalic acid reacted with NH_4F to produce HF and destroy the Ti–Al bond in Ti_3AlC_2 to form multilayers of $Ti_3C_2T_x$ MXene. While chloride ions were inserted in the interlayer of MXenes, the layer spacing increased. Wu and colleagues synthesized a $Ti_3C_2T_x$ MXene with inhomogeneous layering by CoF_2/HCl etching due to the intercalated Al^{3+} and Co^{2+} acting as the backbone of the interlayer spacing of MXene layers.[129] In this study, the effect of the etching environment on the composition, interface, structure and thermodynamic properties of the $Ti_3C_2T_x$ MXenes was investigated. Compared with HF/HCl, CoF_2/HCl etching had more advantages, such as endowing $Ti_3C_2T_x$ MXene with a wider interlayer distance distribution, increasing the number of intercalated cations, and reducing the degree of hydration. In addition, the increased interlayer space, size heterogeneity and reduced hydration led to a reduction in the interlayer van der Waals force interactions and weaker hydration effects. Thus, MXene with intercalated metal cations had a lower exothermic enthalpy (ΔH_f). The results of this work further deepen the understanding of the energy, structure and interface properties of MXene.

MXenes, an emerging and promising class of 2D nanomaterials, have been intensively investigated by researchers since they were first reported in 2011. According to the different requirements of MXene material structure in different application fields, there are many methods to etch MXenes. Although most of the more commonly used etching methods rely on etchants, the use of etchants will have an impact on the etching results to some extent.[130] In addition to the direct HF etching and *in situ* HF etching introduced above, there are many etching methods, such as electrochemical etching, alkali etching, and molten salt etching. In 2021, Luo *et al.* reported a simple one-step molten salt etching method for the preparation of Co-modified MXene.[131] This method was also the first to use a non-fluorochemical method to obtain MXene with the ends completely wrapped in Cl. This experiment proved that the method had the unique advantage of using Cl as T_x, which can effectively improve the electrochemical performance of MXenes.[130] In the case of the electrochemical etching method, it reduces the adverse effects of the etchant on the product given that it avoids the use of an

etchant. Yang *et al.* demonstrated an efficient fluorine-free etching method using anodic etching with Ti_3AlC_2 as the precursor.[132] The etching process was defined by eqn (9), as follows:

$$Ti_3AlC_2 - 3e^- + 3Cl^- = Ti_3C_2 + AlCl_3 \quad (9)$$

The rapid synthesis of MXene at room temperature was achieved by electrochemical etching, and it was also confirmed that the MXene obtained by electrochemical etching has good capacitive performance in all solid-state supercapacitors, indicating that the MXene obtained by this method was superior to that obtained by LiF/HCl etching. The formation of Ti–F bonds and Ti–O bonds during etching indicated the selective etching of Al. By etching with this method, stripped $Ti_3C_2T_x$ nanosheets without any –F terminal functional group could be obtained due to the fluorine-free etching. The use of this method further broadens the application path of MXenes in electrochemistry.

2.3 Functionalization methods of MXenes

MXenes are versatile materials with a wide range of applications due to their surface tunability and terminal chemical activity.[133,134] The surface of MXenes is usually negatively charged due to the presence of –F and –OH groups. Thus, a positively charged compound can be attracted to the MXene surface by electrostatic attraction. For example, positively charged polymers (polyvinylpyrrolidone (PVP) and polyethyleneimine (PEI)) were adsorbed on the surface of MXenes.[135] Generally, the surface of MXenes can be functionalized by electrostatic attraction, physical adsorption and covalent bond formation. Surface functionalization has a direct effect on the electronic state of MXenes, which induces electronic behavior and affects their function.[136] The surface end groups of MXenes also have a significant effect on their physicochemical properties. These surface groups can saturate the non-bonded valence electrons of transition metals through their low-energy orbitals, and thus contribute to structural stability.[137] Consequently, the surface diversity of MXenes can be modulated by controlling the synthesis conditions, such as the chemical potential of different precursors and/or the pH of the solution.[138] In many microporous solid media used as adsorbents or membranes, to overcome the trade-off effect that exists between adsorption capacity (or permeability) and selectivity in separating challenging gas mixtures, scientists have modulated the surface properties of porous media to enhance the interaction of the adsorbent surface with a specific component, thereby increasing the adsorption capacity for the component.[139] Meanwhile, the selectivity can be changed by adjusting the pore size of the solid media, thus providing molecular sieving capabilities, such as carbon molecular sieve (CMS) materials.[140] Previous reports have shown that the surface modification of adsorbents can introduce various functional groups on the adsorbent surface, which can improve the dispersibility and adsorption capacity.[141–143] Taking graphene as an example, graphene has various applications, such as gas sensors, batteries, hydrogen storage and adsorbents.[144–146] For a long time, it has been extensively discussed due to its outstanding adsorption properties. It can adsorb organic compounds, particularly for potential applications associated with common hazardous substances.[147,148] The process of transforming graphene into graphene oxide (GO) through surface modification is relatively convenient and advantageous for different applications.[149] Accordingly, Yu *et al.* prepared GO nanosheets and used them in the biological field for the elimination of the typical antibiotic resistance genes (ARGs). GO nanosheets were effective in removing ARGs due to the high-energy adsorption sites on GO, such as oxygen-containing groups and conjugated Π-sites. In summary, GO has great potential for material functionalization. Several methods for the functionalization of MXenes are presented in detail below.

2.3.1 Hydroxyl group (–OH) functionalization. Hydroxyl groups can provide abundant alkaline sites, which facilitate the adsorption and activation of acidic CO_2 molecules. Consequently, the surface alkalinization of MXenes creates abundant CO_2 adsorption and activation sites, which significantly enhance their activity. Theoretical analysis confirmed that hydroxyl-functionalized MXenes have extremely low work functions, and also demonstrated that the structure of hydroxyl-functionalized MXenes is more stable compared to the pristine MXenes.[150]

In 2018, Wang *et al.* reported for the first time that a titanium carbide (Ti_3C_2) MXene and commercial (P25) were used as a highly efficient non-noble metal co-catalyst for photocatalytic carbon dioxide reduction. The discovery in this work provided a new and highly active alternative to the common non-noble metal auxiliary catalysts for the photocatalytic reduction of carbon dioxide.[151]

MXene and P25, alkalized MXene and P25 were mixed evenly through magnetic stirring to obtain TC/P25 and TC-OH/P25 hybrids, respectively. As shown in Fig. 7a, the characteristic diffraction peaks of TC-OH/P25 were not found in the XRD pattern, which was due to the relatively low mass content of TC-OH in the hybrids and the weak crystallization. In addition, the diffraction peaks in the spectrogram indicated that the mixing of P25 with TC or TC-OH did not change its phase composition and crystal structure. Transmission electron microscopy (TEM) images (Fig. 7b) showed that the P25 nanoparticles were loaded on 2D TC-OH. According to the magnified HRTEM image shown in Fig. 7c, the plane space corresponding to the approximate distance between adjacent lattice stripes shows that there was a close interaction between P25 and TC-OH, which was more conducive to forming a connection between them. The activity of the TC-OH/P25 catalyst was further enhanced compared to TC/P25 due to the modification of TC by hydroxyl groups. As shown in Fig. 7d, 5TC-OH/P25 was 3 and 2.77 times more active than P25 alone for CO and CH_4, respectively. The graph showed the adsorption behavior of CO_2. The absorption of CO_2 by TC-OH at room temperature was significantly higher than that of TC, indicating that the CO_2 molecules were more easily adsorbed on the

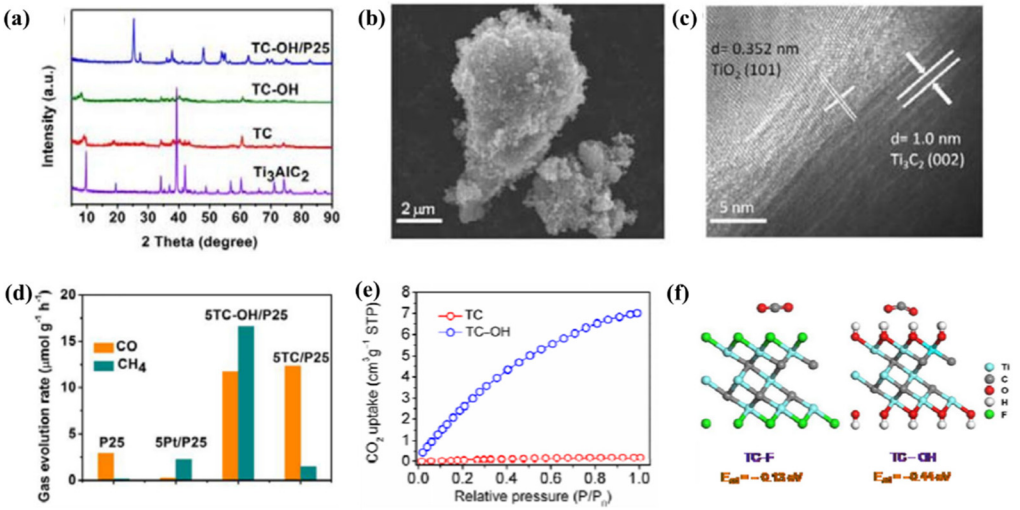

Fig. 7 (a) XRD patterns of Ti_3AlC_2, TC, TC-OH particles and TCOH/P25 hybrids. (b) Typical SEM image of the 5TC-OH/P25 mixture. (c) HRTEM images of the interfacial structure of TC-OH and P25 NPs. (d) Under the irradiation of a 300 W xenon lamp, the release rate of CO and CH_4 on P25, 5Pt/P25, 5TC/P25, 5TC-OH/P25. (e) CO_2 adsorption behavior of TC and TC-OH. (f) Side view of CO_2 adsorption models on 2 × 2 × 1 TC-F and 2 × 2 × 1 TC-OH super-cell. Reprinted with permission.[151] Copyright 2018, John Wiley and Sons.

surface of TC-OH. The adsorption energy of CO_2 on TC-F was −0.13 eV, which was much higher than that of CO_2 on TC-OH of −0.44 eV (Fig. 7e and f, respectively). It is obvious that the higher adsorption capacity of TC-F for CO_2 was due to the lower adsorption energy of CO_2 on TC-OH. In this work, the authors successfully improved the photocatalytic CO_2 reduction activity of P25 by using the Ti_3C_2 MXene, a cocatalyst without noble metals. In particular, the surface alkalinization of Ti_3C_2 MXene further significantly improved the photocatalytic activity and the selectivity for CH_4 release. The data showed that alkalization of the MXene could make its surface functional and significantly improved its performance in applications.

Furthermore, Sun *et al.* prepared multilayer $Ti_3C_2T_x$ MXene by selectively etching the Al layer of Ti_3AlC_2 with hydrofluoric acid according to the literature. Then, the alkaline intercalation of the $Ti_3C_2T_x$ MXene was completed by magnetic stirring, filtering, washing and drying with LiOH, NaOH and KOH solutions, respectively. Finally, three types of alkylated MXene, LiOH–$Ti_3C_2T_x$, NaOH–$Ti_3C_2T_x$ and KOH–$Ti_3C_2T_x$, were synthesized.[152] In this work, some of the alkali-treated $Ti_3C_2T_x$ MXenes were characterized and their adsorption properties for dyes were examined. As shown in Fig. 8a and b, the low peak width intensity in the XRD spectrum of pristine $Ti_3C_2T_x$ showed that the Al in Ti_3AlC_2 was etched, leading to reduced crystallinity. After treatment with LiOH, NaOH and KOH, the characteristic peaks of $Ti_3C_2T_x$ became significantly stronger. In addition, the (002) peak at 9.0° obviously shifted to a lower angle, which indicated that the introduction of additional ion pairs in $Ti_3C_2T_x$ not only expanded its structure, but also increased the uniformity of the lamellae, especially NaOH–$Ti_3C_2T_x$ and KOH–$Ti_3C_2T_x$. As shown in Fig. 8d(i–iii), the SEM micrographs of Ti_3AlC_2 and $Ti_3C_2T_x$ clearly showed that the morphology of Ti_3AlC_2 changed from a dense layer structure to a stacked sheet material with different thickness after HF solution etching. The thickness of the sheets of the Alk-$Ti_3C_2T_x$ lamellar structure varied widely, and the SEM image of LiOH–$Ti_3C_2T_x$ showed that the sheets were stacked but had many large gaps; the thickness of the NaOH–$Ti_3C_2T_x$ sheets was similar to that of the original $Ti_3C_2T_x$; and the multilayer sheets of KOH–$Ti_3C_2T_x$ were not only thicker but also had narrow stacking gaps (Fig. 8d(iv–vi)). The different MXene forms may also affect the adsorption properties for dyes. As shown by the HRTEM images in Fig. 8e–h, the pristine $Ti_3C_2T_x$ was multilayered and the monolayer thickness of MXene increased after the alkalization treatment due to the intercalation of alkali metal ions. Fig. 8c showed that with time, all three types of Alk-$Ti_3C_2T_x$ had a faster MB removal rate than the pristine $Ti_3C_2T_x$. This work demonstrated that Alk-$Ti_3C_2T_x$ obtained by alkaline treatment could significantly expand the layer spacing of MXenes and its surface functional groups were transformed, thus improved the adsorption capacity of MXenes.

2.3.2 Amino ($-NH_2$) functionalization. The surface of MXenes can be functionalized, providing a wider design space for their exploration. Research has showed that the introduction of amino terminal groups on the surface of MXenes for their functionalization can produce MXene-based films with higher performance, which is also an effective strategy to improve their performance.

Xu *et al.* successfully introduced amino end groups on the surface of Ti_3C_2 MXene using a simple sealed thermal method, in which the amination process mainly replaced the hydroxyl groups on the surface of the pristine MXene with amino groups.[153] In this work, the Ti_3C_2 MXene was obtained by etching Ti_3AlC_2 powder with LiF/HCl solution. Then,

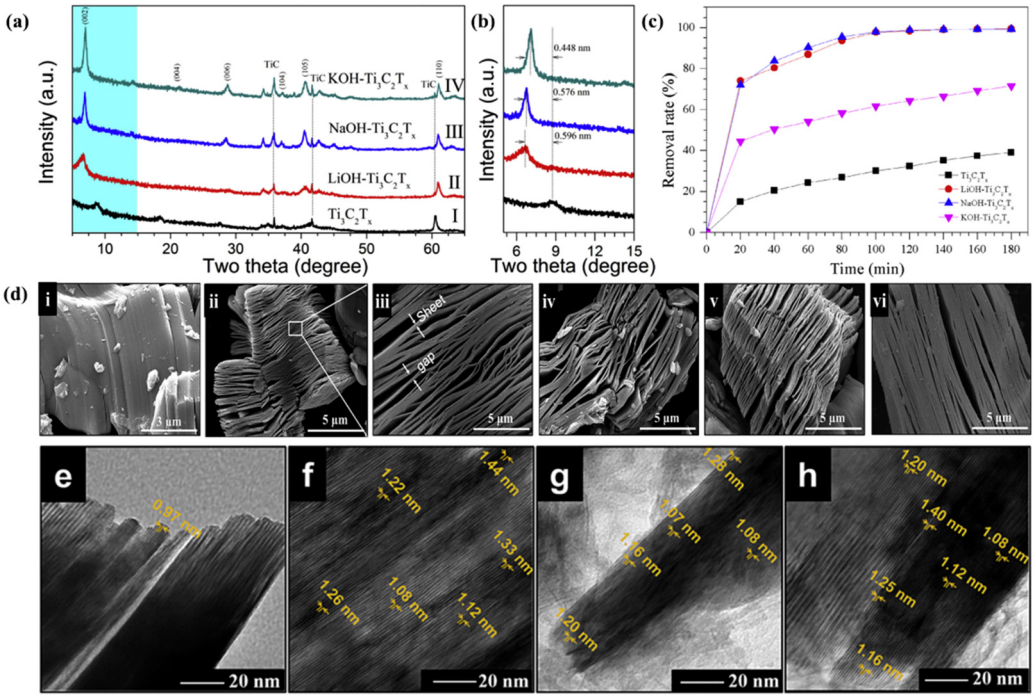

Fig. 8 (a) XRD spectra of $Ti_3C_2T_x$ under different alkaline treatments: (I) $Ti_3C_2T_x$, (II) LiOH–$Ti_3C_2T_x$, (III) NaOH–$Ti_3C_2T_x$, and (IV) KOH–$Ti_3C_2T_x$. (b) Enlarged view of the XRD spectrum in (a). (c) Curves of the removal rate of MB with time for different absorbents. (d) SEM images of Ti_3AlC_2, $Ti_3C_2T_x$ and various Alk-$Ti_3C_2T_x$: (i) Ti_3AlC_2, (ii) $Ti_3C_2T_x$, (iii) enlargement of (b), (iv) LiOH–$Ti_3C_2T_x$, (v) NaOH–$Ti_3C_2T_x$, and (vi) KOH–$Ti_3C_2T_x$. HRTEM images of $Ti_3C_2T_x$ and various alkalized $Ti_3C_2T_x$: (e) $Ti_3C_2T_x$, (f) LiOH–$Ti_3C_2T_x$, (g) NaOH–$Ti_3C_2T_x$ and (h) KOH–$Ti_3C_2T_x$. Reprinted with permission.[152] Copyright 2018, Elsevier.

ammonia water with a certain pH was added to the obtained MXene, it was shook well, and then ultrasonicated and centrifuged. Next, the Ti_3C_2 MXene suspension containing a few amination layers was placed in the reaction still and heated at 70 °C for 4 h. Finally, it was washed and centrifuged to neutral, and the obtained precipitate was freeze-dried to obtain MXene-NH_2 nanosheets (Fig. 9a). The AFM and TEM images showed that the MXene-NH_2 nanosheets were not only uniform in size and thickness but also ultra-thin (Fig. 9b and c). In the XRD spectra, the shift in the (002) characteristic peaks indicated a decrease in the *d*-spacing of MXene-NH_2 compared to the pristine MXene, verifying the change in the morphology and chemical composition of the pristine MXene and MXene-NH_2 nanosheets (Fig. 9d). As shown in Fig. 9e, the UPS spectra of the conventional MXene and MXene-NH_2 nanosheets confirmed that the electron transport behavior of MXene-NH_2 films was still higher, although the work function of MXene-NH_2 increased. Likewise, the conductivity of the pure MXene-NH_2 film reached 21 100 S m^{-1}, but it was reduced by 82.5% compared to the conductivity of the conventional MXene film; nevertheless, its value was still quite large (Fig. 9g). The high conductivity of the MXene-NH_2 film indicated its high electric power supply and good electromagnetic interference shielding effect (SE). The EMI SE value of the pure MXene-NH_2 film in the X-band exceeded 60 dB. Compared with pure traditional MXene films, the EMI SE of MXene-NH_2 was only 5 dB lower, which shows its application potential (Fig. 9f). As shown in Fig. 9h, the CMC molecule had strong mechanical properties due to the formation of hydrogen bonds between it and conventional MXenes. When the CMC molecules and MXene-NH_2 nanosheets formed a thin film, stronger covalent bonds were formed between them in addition to the normal hydrogen bonds, which made the CMC/MXene-NH_2 film simultaneously exhibit excellent flexibility, thus enhancing the tensile properties of CMC/MXene-NH_2, and its mechanical properties were also improved. In summary, all these results indicate that the introduction of amino terminals on the surface of Ti_3C_2 MXene endows it excellent mechanical properties, which not only optimizes the properties of the original product, but also further expands its application scope.

Zhang *et al.* considered that the lack of active adsorption sites definitely affects the adsorption performance of ordinary MXene adsorbents, and thus it is necessary to functionalize the surface of MXenes to optimize their performance. In this work, the researchers prepared a novel MXene-based adsorbent (Ti_3C_2-SL) by combining Ti_3C_2 terminated with a conjugated amino group and sodium lignosulfonate through a simple substitution reaction with hexachlorocyclotriphosphonitrile (HCCP) as the linkage point.[154] Through detection, Ti_3C_2-SL could be used as an adsorbent to adsorb doxorubicin hydrochloride (DOX). Experiments showed that Ti_3C_2-SL could adsorb DOX rapidly and its adsorption amount was significantly higher than that of the unmodified Ti_3C_2, which was

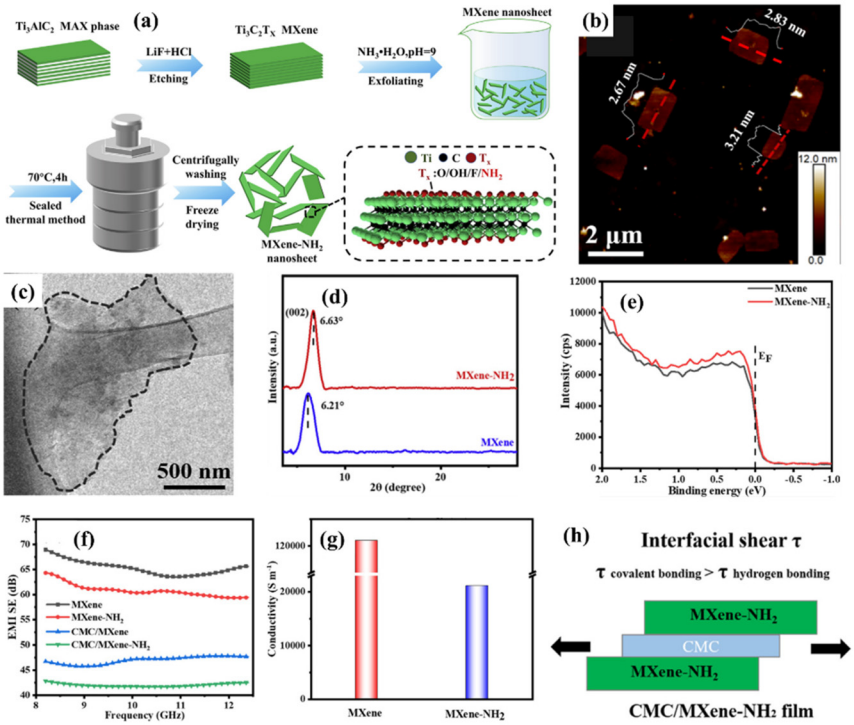

Fig. 9 (a) Schematic diagram of the preparation of aminated Ti_3C_2 MXene. (b) AFM images and (c) TEM images of MXene-NH_2 nanosheets. (d) XRD patterns of conventional MXene and MXene-NH_2 films. (e) UPS spectra of valence band region of conventional MXene and MXene-NH_2 nanosheets. (f) EMI SE of each thin film in the X-band. (g) Electrical conductivity of MXene and MXene-NH_2 films. (h) Schematic diagram of mechanical property enhancement mechanism. Reprinted with permission.[153] Copyright 2021, Elsevier.

about four times that of the original Ti_3C_2. Furthermore, Ti_3C_2-SL had a good application prospect in removing environmental pollutants due to its simple preparation process and significant performance enhancement, and thus this work will significantly advance the environmental applications of MXene-based composites.

Soroush *et al.* used [3-(2-aminoethylamino)-propyl] trimethoxysilane (AEAPTMS) for the amino functionalization of the surface of $Ti_3C_2T_x$ MXene.[155] In this work, the functionalization of MXene caused its zeta potential to change from −35 mV to +25 mV at neutral pH, and this change in the potential caused the MXene able to prepare self-assembled films *in situ*. The results of this work showed that AEAPTMS-$Ti_3C_2T_x$ is a pH-responsive nanomaterial due to the existence of amino groups on its surface and its ability to adsorb or desorb protons with a change in pH.

Besides, in the work by Zhang and colleagues, it was reported for the first time that MXenes ($Ti_3C_2T_x$) and levodopa (DOPA) could be prepared as MXene-based polymer composites ($Ti_3C_2T_x$-PDOPA) after simple mixing under rather mild reaction conditions.[156] In the reaction system, as DOPA can adhere to the surface of MXenes by self-polymerization, resulting in the ability to introduce multiple carboxyl groups during the polymerization process and formation of poly-(DOPA). The resulting $Ti_3C_2T_x$-PDOPA composite was used as an adsorbent, which not only possessed a higher adsorption capacity for heavy metal ions than the pristine $Ti_3C_2T_x$, but could also be further functionalized with other functional materials through subsequent reactions. Because the functionalization of pristine MXenes leads to the introduction of many reactive groups, a variety of composites based on MXenes can be prepared.

Briefly, the amine functionalization approach not only extends the scope of MXenes for more applications in different fields, such as fuel cells, dye adsorbents and antimicrobial coatings, but is also applicable to other MXene structures and composites.

2.3.3 Sulfonic acid group (–SO_3H) functionalization. Wang *et al.* successfully grafted poly-(diallyldimethylammonium chloride) on the surface of Ti_2CT_x MXene nanosheets to improve the stability of Ti_2CT_x MXene by this functionalization method, and the product was used to remove peroxides from a radioactive waste stream.[120] Additionally, sulfonic groups can also be used for the functionalization of MXenes to improve their performance in applications. Researchers have used different methods to combine sulfonic acid groups with MXenes, and the products are gradually being applied in multiple fields.

Because of the rapid development of industrialization, the depletion of fresh water resources is significant.[157] It is well known that the wastewater produced by the dyeing industry has a complex composition and mainly contains dyestuffs with a high salt content, making wastewater treatment complicated and challenging.[158–161] Therefore, various methods have been studied and developed to treat the wastewater generated from printing and dyeing. Zhang *et al.* reported that Ti_3C_2

nanosheets were obtained by etching Al from the Ti_3AlC_2 MAX phase by *in situ*-forming HF etchant, and the surface of the Ti_3C_2 nanosheets was modified with sulfonic acid groups through the direct reaction of diazonium salt and Ti_3C_2 sheets, as shown in Fig. 10a.[162] Meanwhile, the adsorption behavior and adsorption capacity of Ti_3C_2 and functionalized Ti_3C_2 on methylene blue (MB) were further investigated and compared in this work. The SEM images showed that the pristine Ti_3C_2 was a multi-layer 2D nanomaterial with a packaged and stacked lamellar structure, and the interlayer spacing was about 200 nm (Fig. 10d). The apparent granular-structured surface is shown in Fig. 10e, which was due to the modification of Ti_3C_2 by the aryl diazonium salt, that is, the benzene sulfonic acid group functionalized the surface of Ti_3C_2. The comparison of the TEM images of the pristine Ti_3C_2 and Ti_3C_2–SO_3H showed that the transparency of the nanosheets was further improved after surface modification (Fig. 10f and g). The presence of sulfur was observed in the XPS spectra of both samples (Fig. 10b), where the vibrational peaks caused by the asymmetric stretching of the S=O band appeared at 1211 and 1130 cm^{-1} in the FT-IR spectra (Fig. 10i). Furthermore, the weight loss of more than 50% of Ti_3C_2–SO_3H was observed in the TGA curves (Fig. 10j), and the (002) peak was sharpened and shifted to a lower angle in the XRD spectra (Fig. 10h), indicating that Ti_3C_2 was successfully sulfonated by benzene sulfonic acid. As shown in Fig. 10c, compared with the adsorption capacity of the virgin Ti_3C_2 MXene of 21.10 mg g^{-1} for MB in water, that of the benzene sulfonic acid group-functionalized MXene for MB in water was 111.11 mg g^{-1}, which is five times higher than that of the pristine MXene. This study demonstrated that Ti_3C_2–SO_3H is a promising and efficient adsorbent for the removal of organic dyes from the aqueous environment.

Pu *et al.* embedded sodium lignosulfonate (LS), which contained abundant hydrophilic groups (sulfonic acid groups and phenolic hydroxyl groups), and MoS_2 nanosheets in MXene nanosheets for functionalization.[163] The researchers prepared 2D MoS_2@LS-MXene composite membranes with high water permeability and outstanding dye separation properties *via* the pressure-assisted self-assembly technique, as shown in Fig. 11a. The MXene nanosheets added with deionized water were ultrasonically dispersed, and after the dispersion was uniform, LS was added with magnetic stirring for a certain time, resulting in the functionalization of the MXene nanosheets. Subsequently, specific concentrations of MoS_2 dispersion liquid were added for sonication to obtain precursor solutions of different compositions, after which MXene-based composite films were prepared. The hydrophilicity and permeability of the membranes were tested by water contact angle (CA) and pure water flux measurements (Fig. 11c). Given that LS is a biological macromolecule containing sulfonic acid groups and many phenolic hydroxyl groups, it endowed the prepared composite membranes with good hydrophilic properties. Consequently, with an increase in LS content, the water contact angle of the composite film decreased, indicat-

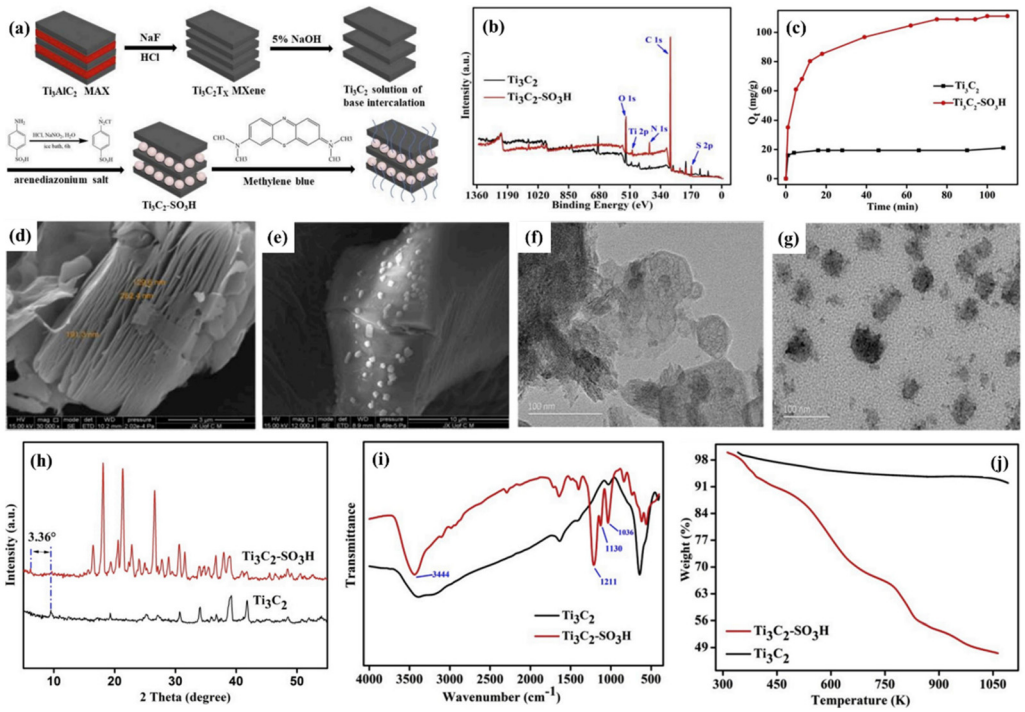

Fig. 10 (a) Schematic diagram of the preparation of Ti_3C_2 and Ti_3C_2–SO_3H. (b) XPS wide scan spectra of pristine Ti_3C_2 and Ti_3C_2–SO_3H. (c) Effect of contact time on the adsorbed MB on pristine Ti_3C_2 and Ti_3C_2–SO_3H. SEM images of (d) virgin Ti_3C_2 and (e) Ti_3C_2–SO_3H. TEM images of (f) virgin Ti_3C_2 and (g) Ti_3C_2–SO_3H. (h) XRD patterns of virgin Ti_3C_2 and Ti_3C_2–SO_3H. (i) FT-IR spectra of virgin Ti_3C_2 and Ti_3C_2–SO_3H. (j) TGA curves of virgin Ti_3C_2 and Ti_3C_2–SO_3H. Reprinted with permission.[162] Copyright 2019, Elsevier.

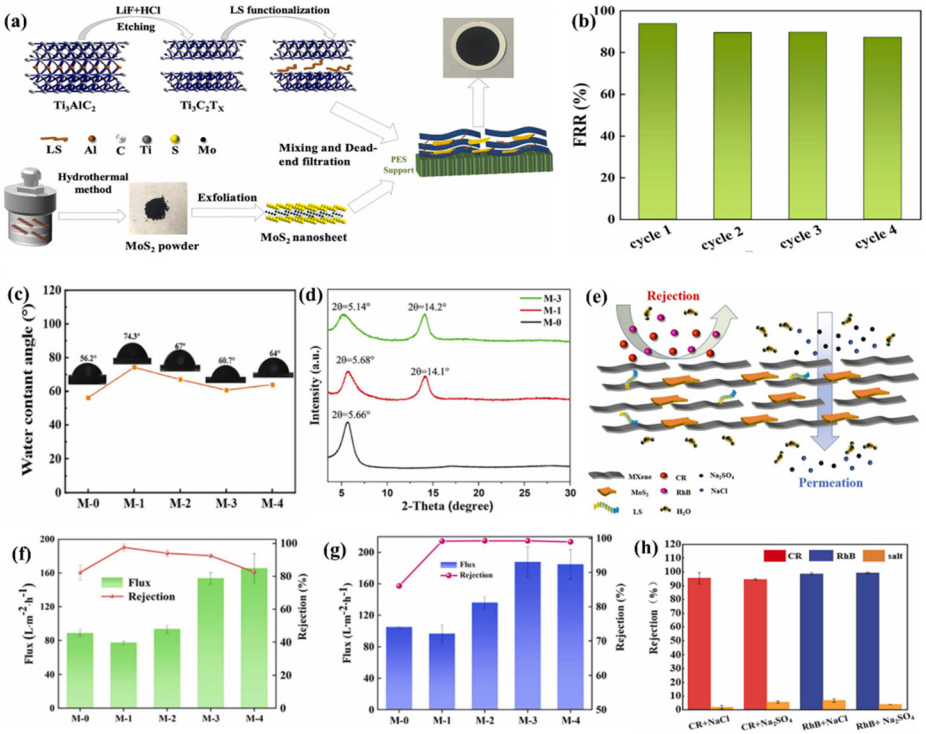

Fig. 11 (a) Scheme for the preparation of MoS_2@LS-MXene composite films by pressure-assisted self-assembly. (b) FRR data of M-3. (c) CA of all membranes. (d) XRD patterns of M-0, M-1, and M-3. (e) Separation mechanism of MoS_2@LS-MXene composite membranes. Removal rates of dyes by different membranes: (f) CR and (g) RhB, and (h) separation of dye/salt mixture with M-3. Reprinted with permission.[163] Copyright 2022, Elsevier.

ing an increase in hydrophilicity. The enhanced hydrophilicity also improved the breathability of the membrane. Because the membrane with hydrophilic surface could prevent the accumulation of contaminants in water on its surface, its antifouling ability was improved. The XRD patterns of the three samples showed (Fig. 11d) that the (002) peaks of the MXene nanosheets after LS treatment were not only broadened but also shifted to a lower angle, indicating an increase in the layer spacing of the composite films. The increased interlayer spacing and hydrophilicity provided a suitable environment for the rapid permeation of water molecules, indicating that the water flux of the composite membrane became larger. As shown in Fig. 11f and g, to examine the separation performance of the MXene composite membranes, the researchers used Congo red and rhodamine B to simulate dye wastewater vapors. It was clearly observed that the layer spacing of the MXene composite membranes increased with an increase in LS content, and the removal rates of CR and RhB were improved for all the membranes. The composite membranes removed both Congo red and rhodamine B in mixed solutions at more than 95% compared to the single component dyes (Fig. 11h). The result showed that the MXene composite membranes had a good performance for dye/salt separation. In addition, the composite membrane could be recycled again after washing, and the recycling also showed that the composite membrane had good flux recovery performance. Fig. 11b shows the flux recovery of the M-3 membrane after CR permeation and DI water cleaning. It can be seen that the flux of the composite membrane still recovered well when cleaned with detergent for 10 min at each cycle. Also, the separation mechanism of the composite membranes showed that when the composite membranes had an appropriate interlayer spacing, smaller-sized saline hydrated ions could permeate them, while larger-sized dye molecules were repelled, thus achieving mutual separation (Fig. 11e). The functionalized composite films obtained in this work not only exhibited good stability and fouling resistance, but this study also provided novel design ideas for the preparation of high-performance materials.

In summary, it is not difficult to see that there are numerous ways to functionalize MXenes. In addition to functionalization with surface groups, it is also possible to functionally optimize the defects of MXenes with substances that are also 2D materials.[163] It is sufficient to prove that the products obtained from the functionalization of MXenes have excellent performance, which not only broadens the application direction and field of MXenes, but also makes MXenes extremely potential for development.

3 MXene-based gas separation membranes and their structure–performance relationships

Molecular sieve fractionation membranes are ideal as efficient gas separation materials, and to achieve the ideal gas separ-

ation effect, it is recognized that they should have sufficient and homogeneous nanochannels. Accordingly, the use of 2D materials, such as graphene, GO, and MOF nanosheets, provides many innovative design ideas for the design of gas separation membranes.[164–166]

3.1 MXene-based gas separation membranes

Considering the prominence of environmental problems, the cost of energy in production and life is increasing, increasing attention is given to sustainable development and improving the energy utilization efficiency, and thus energy-saving membranes have attracted extensive attention in different fields. Nanoporous membranes possess excellent molecular sieving mechanisms due to their uniform and sufficient nanochannels, which breaks the trade-off between permeability and selectivity in gas separation, and thus facilitates efficient gas separation.[167] MXenes have high efficiency and energy saving separation properties due to their structure and special chemical surface, and the modifiable properties allow the membranes prepared from them to exhibit superior performance in various separation sciences. Consequently, MXene-based membranes are increasingly being used in high-performance separation/purification.[77]

Well-designed methods for the preparation of membranes are essential to achieve the goal of efficient separation processes. According to the actual needs, great progress has been achieved in the past few years by combining different methods to design membranes accurately and rationally. Under vacuum filtration conditions, the fabricated membranes form nanochannels of different lengths and widths due to the high aspect ratio of MXenes, and these nanochannels provide pathways for gas diffusion (Fig. 14c).[168] Consequently, changing the interlayer distance and length of the nanochannels will allow different types of gases to pass through the membrane and also change the gas permeability, which in turn will achieve the purpose of gas separation. In MXene separation membranes, CO_2 will be adsorbed in the MXene nanochannels, which prevents its transport, thus capturing CO_2.[85] MXenes have been progressively combined with stand-alone or film-composite polymers to prepare separation membranes. This method can increase the affinity between CO_2 and the matrix. Because the nanochannels formed by MXene nanosheets contribute to molecular sieving and provide a more tortuous path for gas transport in the membrane, MXene-based gas separation membranes can improve the selectivity and permeability of the corresponding MXene MMMs.[77] Compared with other existing 2D separation membranes (such as ZIFs and MOFs), MXene-based membranes may have the same selectivity and higher permeability. In addition, research has shown that lamellar MXene-based films exhibit excellent reproducibility, good mechanical properties, and stable separation performance due to their ordered nanochannels in the long-term continuous separation process.[75]

As shown in Fig. 12a, $Ti_3C_2T_z$ MXene was embedded in Pebax-1657 block copolymer in the work by Ahmad *et al.* The mixture of these two substances formed good nano-channels to achieve the fast and selective transport of CO_2, and the mixed matrix membrane also showed an excellent CO_2 separation performance. Besides, the experimental scheme of mixing the MXene and polymer in the experiment could also mitigate the oxidation of the MXene.[85] In the work by Li and colleagues, the $Ti_3C_2T_x$ MXene was combined with Pebax to prepare a mixed matrix membrane for the separation of CO_2.[169] According to the scanning electron microscopy images of the cross section of the membranes, as shown in Fig. 12f and g, the MXene in the matrix was uniformly dispersed at 1% loading, while the cross-section was relatively smooth at 5% loading. The FTIR spectrum of the Pebax-MXene films, which characterized the interaction between the filler and the matrix, showed a slight shift in the peaks for the Pebax-MXene films at 3302 cm^{-1} and 1640 cm^{-1}. The shift in these bands suggested that the interaction between the surface end groups of MXene and the Pebax chain may be hydrogen bonding (Fig. 12b–d). As shown in Fig. 12e, the CO_2 permeability of the Pebax-MXene membrane was significantly greater in the wet state than in the dry state, and this state was related to the fact that the membrane swelled when wet. When the content of MXene in the membrane increased from 2% to 5%, the CO_2/N_2 selectivity of the membrane in the wet state clearly tended to increase, which was obviously different from the trend in the dry state. However, in general, Pebax-MXene membranes exhibit a high separation performance due to the abundance of functional groups on the MXene surface.

In addition to the above-mentioned separation membranes prepared using MXenes and polymer Pebax, other MXene-based membranes have also been extensively used in the field of gas separation. According to the outstanding structural characteristics and unique chemical surface of MXenes, researchers have designed MXene-based films combined with different substances. For example, Ding *et al.* used vacuum-assisted filtration in a laboratory study to place MXene nanosheets on anodic aluminum oxide carriers and could separate the MXene films "independently". Furthermore, it was reported that the peeled MXene films showed good flexibility.[75] Li and colleagues conducted an in-depth study on gas diffusion in MXene interlayer nanochannels through MD simulations to understand the selective diffusion of gases in MXene interlayer nanochannels at the molecular level. In this work, the diffusion behavior of many different gas molecules in MXene membranes with different structures was investigated, and the results showed that the effect of different MXene membrane structures on gas diffusion was significant.[170]

Furthermore, functional liquids, such as ionic liquids (IL), have the ability to achieve the purpose of separating different gases and enclosing undesirable defects in the packing due to their different solubility based on gases. Therefore, it is a very effective method to embed them in 2D layered membranes for the separation of gases with similar kinetic diameters. Considering this, Li *et al.* used a simple method to sulfonate MXene, followed by embedding the typical ionic liquid 1-butyl-3-methylimidazolium tetrafluoroborate ([BMIM][BF_4]) in the

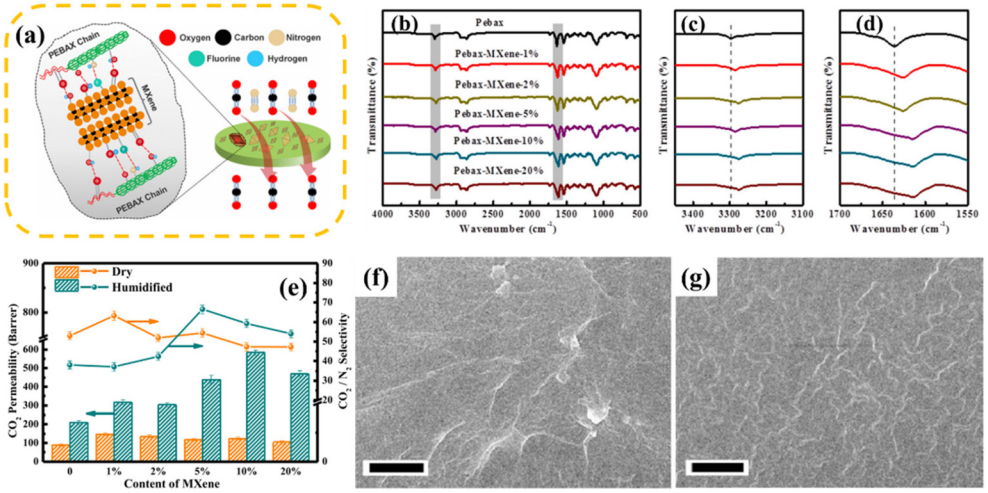

Fig. 12 (a) Design of Pebax/MXene membrane. Reprinted with permission.[85] Copyright 2020, the American Chemical Society. (b)–(d) FTIR spectrum of Pebax-MXene films. (e) Gas transport characteristics of Pebax-MXene films under dry and wet conditions. (f) Cross sectional scanning electron microscopy images of Pebax-MXene-1% membrane and (g) Pebax-Mxene-5% membrane. Reprinted with permission,[169] Copyright 2021, Elsevier.

ionized nanochannels of the sulfonated MXene nanosheet lamellar membrane to separate CO_2 and N_2 molecules.[171] In this work, inspired by catechol-metal chelation, $Ti_3C_2T_x$ MXene nanosheets containing a large number of unsaturated Ti atoms were chosen as the main building blocks to facilitate the homogeneous introduction of sulfonic acid groups ($-SO_3H$). Also, a method of ionization was proposed, *i.e.*, the modification of the nanochannels of the lamellar membrane with disodium 4,5-dihydroxy-1,3-benzenedisulfonate, which is a catechol derivative. The method allowed the IL to be stably immobilized in the nanochannels and achieved effective separation of CO_2. The membranes prepared using the MXene modified by sulfonic acid groups had intrinsic advantages compared to previously reported liquid-immobilized lamellar membranes.[172] The membrane with the best performance had a certain interlayer spacing and high absorptivity for IL, endowing it with high permeability to CO_2 and high selectivity for CO_2/N_2. Besides, the IL loss rate of the membranes prepared by growing sulfonic acid groups in the nanochannels of MXene under high pressure (5 bar) significantly decreased within seven days compared to the unsulfonated MXene, indicating that the MXene functionalized with sulfonic acid groups showed good stability for IL storage. In conclusion, the membranes reported in this work not only had comparable permeate flux and stability, but also were expected to contribute to the development of liquid-based membranes.

In 2022, Wei *et al.* first reported the preparation of a free-standing MXene-ZIF-8 bilayer hydrogen separation membrane.[173] To achieve MXene layer assembly and ZIF-8 growth, the researchers combined electrophoretic deposition (EPD) and fast current-driven synthesis (FCDS). As shown in Fig. 13a, this method resulted in the synthesis of independent MXene-ZIF-8 bilayer composite membranes in a relatively short period, enabling the simple and rapid production of membranes, while overcoming the time-consuming drawback of the traditional vacuum filtration and thermal synthesis methods. This figure showed that the thinner 2D layered MXene was obtained in a short time through EPD. Secondly, based on the MXene layer as the conductive substrate, a certain thickness of ZIF-8 layer was rapidly grown on the MXene layer using FCDS. The final MXene-ZIF-8 bilayer composite membrane could be used as a suspension membrane for gas separation. In the experiment, a single gas permeation test was performed for the MXene membrane and MXene-ZIF-8 bilayer composite membrane. The results indicated that the H_2/CO_2 selectivity of the pure MXene membrane exceeded the Knudsen selectivity, and the permeability of N_2 and CH_4 was higher than that of CO_2 due to the adsorption of CO_2 by the MXene (Fig. 13c). The MXene-ZIF-8 bilayer composite membrane, which grew a ZIF-8 layer, showed an almost twofold increase in H_2/CO_2 selectivity and a nearly threefold improvement in H_2/C_3H_8 selectivity compared to the pure MXene membrane (Fig. 13d). This suggested that the combination of MXene nanosheets layer with ZIF-8 helped to improve the gas separation performance of the membrane. As shown in Fig. 13e, the gas separation performance curve of the MXene-ZIF-8 bilayer composite membrane for H_2/CO_2 at different temperatures clearly showed that the CO_2 permeability increased with an increase in temperature. Subsequently, the researchers conducted a long-time H_2/CO_2 separation test on the MXene-ZIF-8 bilayer composite membrane, and the results showed that its permeability for H_2 and CO_2 remained almost unchanged during more than 100 h of operation. Simultaneously, the H_2/CO_2 selectivity was only slightly reduced, which confirmed the excellent stability of the MXene-ZIF-8 double-layer composite membrane (Fig. 13f). In addition, the excellent crystal structure of the ZIF-8 layer, the SEM image of the tightly bound MXene-ZIF-8 bilayer, and the elemental mapping of Zn and Ti in the MXene-ZIF-8 bilayer composite film indicated that the composite films still had a satisfactory and stable structure after long-time gas separation

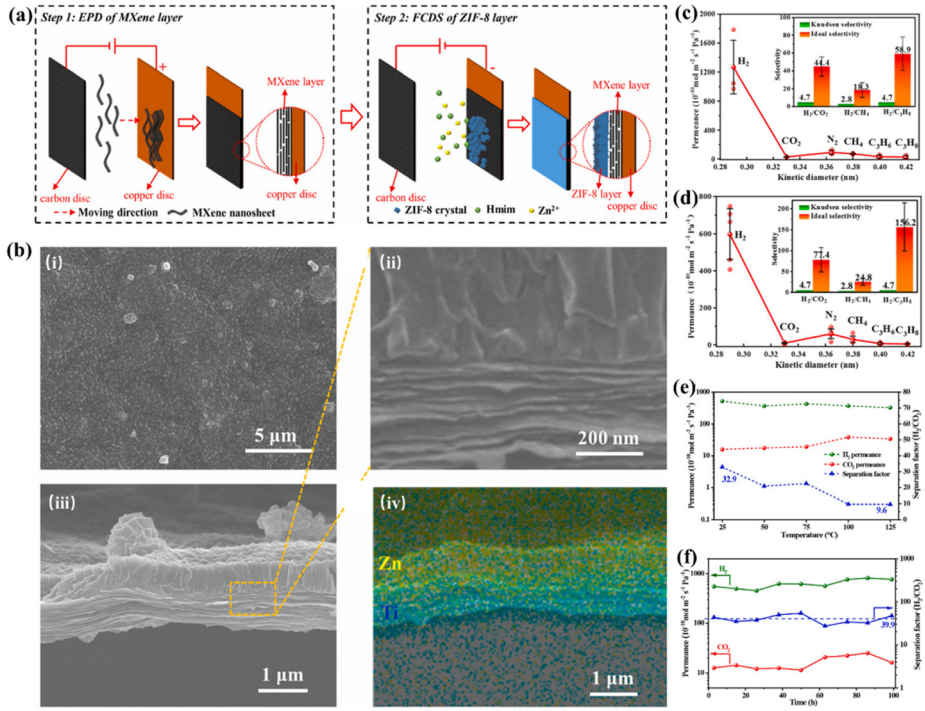

Fig. 13 (a) Schematic diagram of the rapid synthesis of MXene-ZIF-8 bilayer composite membrane. (b) (i)–(iii) SEM images of the ZIF-8 layer, MXene layer interface and MXene-ZIF-8 bilayer composite film cross-section; (iv) are elemental mappings of Zn and Ti corresponding to (iii). Single gas permeability and selectivity of (c) MXene membranes and (d) MXene-ZIF-8 bilayer composite membranes. (e) Separation performance of MXene-ZIF-8 bilayer composite membranes for H_2/CO_2 mixtures at different temperatures. (f) Long-term separation performance of MXene-ZIF-8 bilayer composite membranes for H_2/CO_2 mixtures. Reprinted with permission.[173] Copyright 2022, Elsevier.

(Fig. 13b). The MXene-ZIF-8 bilayer composite membrane prepared in this work had the advantages of high synthesis efficiency, superior H_2/CO_2 selectivity, and extremely fast membrane preparation time. Simultaneously, the concept of designing membrane structures can be extended to other double-layer membranes, which provides a new idea for the development of membrane preparation.

In summary, with the increasing in-depth research on MXenes, there are more in-depth studies and innovative design ideas for the preparation of MXene-based gas separation membranes, which further illustrates the application and development potential of 2D nanomaterial MXenes in gas separation membranes.

3.2 Structure–property relationship of MXene-based gas separation membranes

Considering the wide application of MXene-based membranes in the field of high-performance separations/purification, it is not difficult to find that the design of MXenes with excellent stability and specific functionality is essential to achieve efficient separation. Gas permeation within MXene membranes is similar to other 2D layered membranes and can occur in three different regions, as follows: (i) in-plane crack-like pores formed by nonstructural defects between adjacent MXene sheets; (ii) interplanar interlayer pore channels, which can be controlled by the coating method and functional groups; and (iii) voids in poorly ordered MXene layers observed in graphene oxide and other 2D material membranes (Fig. 14a and b).[174,175] Under vacuum filtration condition, MXene nanosheets with a high aspect ratio can form nanochannels (interlayer spaces between parallel nanosheets) and nanoliths (voids between the edges of the nanosheets) in the prepared membranes (Fig. 14c). The nanochannels not only provide diffusion pathways for gas transport, but their different interlayer spacings can also allow different gas permeability through the membrane.[168] Because the layered MXene-based films have aligned nanochannels and many surfaces end groups on the adjacent MXene nanosheets, MXene-based films possess superior CO_2 capture performance.[75] However, different MXene membranes structures (*e.g.*, species of intercalating ions and interlayer distance) have a large degree of influence on the diffusivity of the gas.[170] Thus, to solve these problems and synthesize the target MXene membrane, several influencing factors need to be considered. For example, the surface functionalization and adjustment of the interlayer spacing of MXene layers, as mentioned in section 2, as well as the intercalation of MXene layers or by combining them with other 2D materials to optimize the surface defects of the MXenes themselves, as described below.

3.2.1 Surface modification of MXenes. The interlayer spacing and surface termination of MXenes have a substantial impact on the gas separation performance of the membrane.

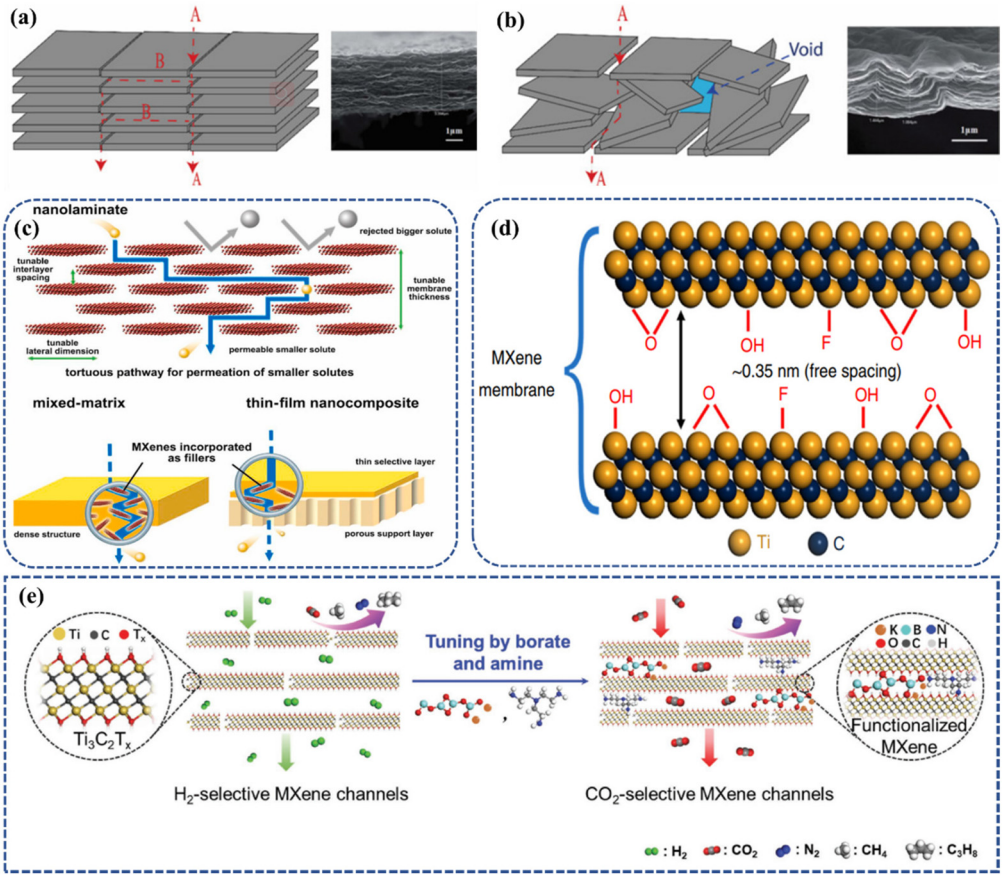

Fig. 14 Schematic diagrams of two mass transport mechanisms (a) through in-plane fissure-like pores (A) and interlayer channels (B). (b) Voids formed between the less ordered MXene nanosheets. Reprinted with permission.[176] Copyright 2022, the American Chemical Society. (c) Separation mechanism of MXene-based membrane. Reprinted with permission.[77] Copyright 2020, John Wiley and Sons. (d) Schematic diagram of adjacent MXene nanosheets. Reprinted with permission.[75] Copyright 2018, Springer Nature. (e) Schematic diagram of the selective permeation of H_2 and CO_2 in MXene membrane. Reprinted with permission.[73] Copyright 2018, John Wiley and Sons.

Wang *et al.* conducted several studies on MXenes, and the results showed that the nanochannels between the layers of the MXene membranes were similar to that of GO membranes, both of which used the size effect for the purpose of gas separation (Fig. 14d).[75] After their systematic study of the diffusion mechanisms of multiple gases (including H_2, He, CO_2, N_2 and CH_4) in 2D MXene nanochannels, they found that both the structural factors of gas molecules (such as size, mass and polarity) and the structural factors of MXene membranes (such as layer spacing and the presence of water molecules) had significant effects on the diffusion of gases through kinetic simulations.[170] Jin *et al.* modified MXene with boric acid and polyethyleneimine (PEI) to achieve the modification of an MXene assembly and change its layer spacing. As shown in Fig. 14e, the MXene nanosheets were well stacked and the MXene nanochannels were reasonably regulated by the surface functionalization. After the modification, the borate and polyethyleneimine (PEI) molecules were well interlocked in the MXene layer. The results showed that this method finely tuned the stacking behavior and interlayer spacing of the MXene nanosheets. In this work, the unfunctionalized and functionalized MXene nanomembranes were compared and the latter was found to exhibit different stacking behavior and adjustable interlayer spacing, while preferentially allowing CO_2 permeation. Also, the MXene nanomembrane, which was capable of selective transport of H_2 and CO_2, exhibited an outstanding CO_2 separation performance. This study focused on the mechanism of gas transport in the MXene lamellae inside the nanomembrane and revealed that the transport mechanism of the MXene membrane changed from "diffusion control" to "solution control" after chemical adjustment. The idea of preparing MXene nanomembranes through rationally designed tunable nanochannels, which were precisely clipped to modify the 2D nanostructure, inspired the exploration of other nanomaterials, which will further propel the application of 2D nanomaterial membranes.

Due to the fact that the adjacent nanosheets in a 2D layered membrane are usually stacked randomly, they form disordered nanochannels, which can hinder the efficient separation of the target gas. Therefore, it is necessary to fabricate MXene lamellar membranes with regularly arranged and ordered sub-nanochannels. Wang *et al.* prepared $Ti_3C_2T_x$ nanosheets with

lateral dimensions of around 1 μm by improving the method of preparing nanosheets using a mixed solution of LiF and HCl. Then, on an anodic aluminum oxide (AAO) substrate with a pore diameter of 200 nm, a self-supporting membrane was prepared by vacuum-assisted filtration.[75] Because of the abundant surface end groups of the MXene, the membrane exhibited an H_2 permeate flux of 2200 Barrer and H_2/CO_2 selectivity of over 160, a performance that exceeded that of most membrane materials available at the time. The performance achieved to such an extent, in addition to the interaction between the surface end groups and the gas molecules, is also largely dependent on the size sieving effect of the sub-nanometer interlayer channels on H_2 and CO_2.

The above-mentioned work achieved the modulation of MXene interlayer spacing and the stacking mode of interlayer nanosheets through chemical modification and intramolecular interactions (electrostatic interactions, hydrogen bonding and covalent bonding), thus preparing MXene nanomembranes with outstanding CO_2 separation performances.

3.2.2 Cationic intercalation of MXene layers. Unlike the surface chemistry of graphene and its derivatives, monolayer MXene nanosheets bind OH, O and F in aqueous solution to form a T_x cover with homogeneous hydrophilic surface functional groups, which may enable the MXene nanosheets to exhibit a better stacked structure during film formation.[120] In addition, MXenes can be chemically and electrochemically intercalated by monovalent and multivalent metal cations (*e.g.*, H^+, Li^+, Na^+, K^+, Ca^{2+}, Mg^{2+}, Al^{3+}, and NH_4^+) as well as organic molecules.[177–183] The insertion of positively charged ions or small nanoparticles between MXene layers can expand the width of the original nanochannel, thereby increasing the gas flux through the membrane. Because of the different interactions between MXene nanosheets and between the intercalated microclusters, the layer spacing is adjustable. The intercalation of cations of different sizes and charges in the $Ti_3C_2T_x$ interlayer leads to the expansion or contraction of its lamellar structure, and these studies provide a good basis for the layer spacing-regulated sieving performance of MXene 2D films. Multilayer MXenes can be further transformed into monolayer or fewer-layer nanosheets by intercalation and delamination, and the introduction of additional substances in the layered MXene structure by ionic intercalation is another strategy to control its properties.[120]

When the etchant used for synthesizing MXene is different, it also has an effect on the layer spacing of the MXene. For example, when etching MXene with HCl-LiF solution, Li^+ will be interpolated between the MXene layers, thus synthesizing MXene with relatively large lattice parameters.[120] In their work, Wang *et al.* uniformly combined $Fe(OH)_3$ nanoparticles with a diameter of 4–5 nm with the MXene surface by electrostatic interaction, and then removed the excess nanofillers with HCl solution to obtain 2D nanochannels with a layer spacing of 2–5 nm.[184] The MXene membranes obtained by this method showed outstanding permeability and stability. The showed that the width of the MXene nanochannels could be controlled by cationic intercalation, which in turn led to the better performance of the MXene membranes. Meng *et al.* intercalated Ni^{2+} in MXene nanosheet layers, and then assembled the modified MXene nanosheets with Al_2O_3 hollow fibers to form molecular sieve membranes (MSMs) through a vacuum-assisted filtration and drying process (Fig. 15a).[185] The membrane had an H_2 and CO_2 selectivity of 615 and H_2 per-

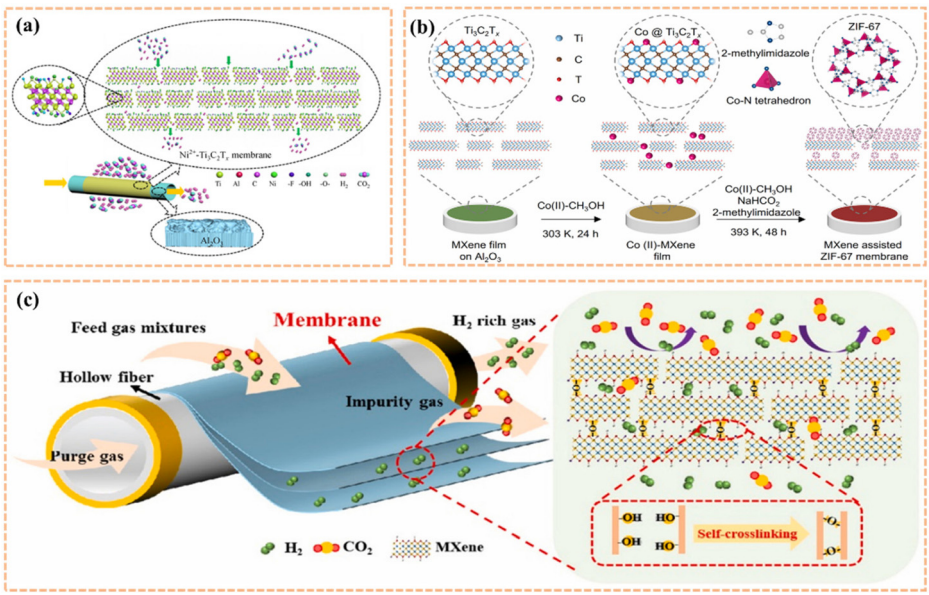

Fig. 15 (a) Schematic diagram of Ni^{2+}–$Ti_3C_2T_x/Al_2O_3$ hollow fiber membrane for separation of hydrogen and carbon dioxide mixtures. Reprinted with permission.[185] Copyright 2020, Springer Nature. (b) Schematic diagram of the preparation of MXene-assisted ZIF-67 film on Al_2O_3 disc. Reprinted with permission.[186] Copyright 2022, Elsevier. (c) Schematic diagram of self-cross-linked MXene hollow fiber membrane for H_2/CO_2 separation. Reprinted with permission.[187] Copyright 2021, Elsevier.

meability of 8.35×10^{-8} mol m^{-2} s^{-1} Pa^{-1} at room temperature. Compared with the $Ti_3C_2T_x/Al_2O_3$ hollow fiber membrane without intercalated cations, due to the strong interaction between the negatively charged MXene nanosheets and Ni^{2+}, the interlayer spacing of the MXene was regulated. Consequently, the selectivity and permeability of the membrane prepared after Ni^{2+} intercalation were significantly improved. Also, the membrane continued to operate for 200 h and still had a stable gas separation performance. This work showed that the $Ti_3C_2T_x/Al_2O_3$ hollow fiber membranes prepared after Ni^{2+} intercalation have a broad prospect for industrial applications.

Because of the abundance of end groups on the surface of MXenes, cation intercalation produces a certain interaction with it, causing the intercalated modified MXene membranes to exhibit more outstanding gas separation performance and stability. Consequently, changing the structure of the MXene layers by cationic intercalation plays a decisive role in the separation performance of the prepared MXene membranes.

3.2.3 MXene combined with other 2D materials. Although MXenes have some unique advantages compared to other 2D materials, the stacked structure of MXene nanosheets may still have non-selective defects that cannot be ignored. For example, Jin *et al.* firstly polymerized highly branched polyethyleneimine-functionalized MXene nanosheets with trimeric chloride by interfacial polymerization to seal the non-selective structure of MXene nanosheets, and then obtained good-performing MXene films.[88] Furthermore, MXenes can be combined with other 2D materials to optimize the separation performance of the prepared membranes to achieve defect complementation. Zeolite imidazolium skeletons (ZIFs) have been used for gas separation for many years due their advantages such as tunable pore structure. ZIF-67 possesses a topology that uses cobalt as a metal node, which is a good material for gas separation. Feldhoff *et al.* combined ZIF-67 with MXene to prepare high-performance gas separation membranes.[186] As shown in Fig. 15b, MXene films were first prepared on an Al_2O_3 substrate, and then Co^{2+} was intercalated in the MXene films to obtain Co(II)-MXene films, and finally ZIF-67 was synthesized under specific conditions in the presence of MXene films and the MXene films were bound to them. Given that Co^{2+} was embedded in the MXene nanosheet layers by adsorption, it led to an increase in the interlayer spacing of the MXene, and therefore the content of Co^{2+} in the intercalated layers of the membrane, which determined the non-homogeneous nucleation and crystal growth of ZIF-67. Thinner ZIF-67 films were prepared with the assistance of Co(II)-MXene films. The results showed that the prepared ZIF-67 membranes with the assistance of MXene not only had exceptional gas selectivity and permeability, but also had good long-term chemical and thermal stability.

The above-mentioned studies showed the potential of combining MXenes with other 2D materials for the preparation of high-performance gas separation membranes. However, thus far, this route has not been widely explored and applied in the field of gas separation. Also, this means that MXenes have a broader scope for development and application in the field of high-performance separation/purification.

3.2.4 Others. In addition to the above-mentioned common methods of slightly modifying MXenes, and then modulating their structure to achieve the enhanced separation performance of MXene-based membranes, other methods, such as by modulating the substances or substrates bound to MXenes, have been reported for the preparation of membranes with excellent properties.

Inorganic hollow fibers are a good substrate for the large-scale preparation of 2D material membranes; however, if 2D materials are inefficiently stacked on hollow fibers, it will lead to an oversized interlayer space and extremely low sieving performance. Xu and colleagues prepared self-crosslinked MXene hollow fiber membranes with good gas separation performance and stability from yttrium-stabilized zirconia (YSZ) hollow fibers *via* a simple heat treatment and self-crosslinking process.[187] As shown in Fig. 15c, the prepared self-cross-linked MXene hollow fiber membranes were capable of forming sieving-capable nanochannels between adjacent MXene nanosheets due to the abundance of end-group groups on the MXene surface. The preparation process resulted in a regular reduction in the interlayer spacing of the MXene films during the heat treatment crosslinking, which led to a significant improvement of their H_2/CO_2 separation performance. Meanwhile, the operational stability of the prepared self-crosslinked MXene/YSZ (SM/YSZ) hollow fiber membranes was highly competitive.

As mentioned above, the structure of MXenes is inextricably linked to their properties and the performance of the prepared membranes. Whether it is the functionalization of MXenes, cationic intercalation, functionalization of other materials or combination with other 2D materials, these are essentially adjustments to the structure of MXenes, especially their interlayer spacing. The structurally altered MXene membranes almost always exhibit superior separation performance and stability compared to the original MXene membranes. However, obviously, there are still relatively few MXene membranes with outstanding performance for gas separation, which indicates that although they have great potential for development, there is still a long way to go for their research and exploration.

4 Summary, challenges and future prospects

It is undeniable that as a new class of 2D nanomaterials, MXenes have unique advantages that cannot be underestimated. They provide a lot of new ideas for the research of gas separation and other fields and have great development potential and promising development prospects. However, presently, research on MXenes is still in the preliminary development stage and there are many challenges to be addressed.

4.1 Summary

Through a thorough understanding of MXenes, it is possible to recognize their unique advantages compared to other 2D materials and the areas in which they can be applied, as well as provide a theoretical basis for their interfacial modulation and structural optimization. After etching MXenes, their surface forms rich functional groups, and the MXene surface functionalized by different methods exhibit an appreciable enhancement in performance, making them advantageous for further applications. Besides, some MXene-based membranes for high-performance separation/purification applications have been presented, illustrating the great application potential of MXene-based membranes and their inextricable structure–performance relationship.

4.2 Challenges

The summary of the related research work showed that MXenes, after surface modification and structural optimization, exhibit greatly improved the pro-CO_2 and adsorption properties, but there are still some problems. Firstly, in the case of their structure and properties, the effects of different structures on the properties of MXenes should be continued to be explored, together with the effects of using different preparation methods on the structure and properties of MXenes. Moreover, the further exploration of other properties of MXenes that have not been discovered before will expand their application areas. Secondly, for the interfacial modulation of MXenes, most of the composites are bonded by certain physical interactions (hydrogen bonding, van der Waals forces, *etc.*) with poor mechanical properties, and thus further exploration of chemical bonding interaction modulation is needed to improve their comprehensive performance. Thirdly, more methods need to be explored to modulate the surface of MXenes to improve their thermal stability, chemical stability and oxidation resistance and to lay the foundation for their multi-disciplinary applications. Finally, based on the existing research on the 2D nanosheet structure of MXenes, we should explore what type of influence mechanism MXenes will have on the performance of composite materials during their application, which will help to deepen and improve the modulation of the performance of MXenes, and then refine their practical application in gas separation and provide a theoretical basis for CO_2 capture and separation.

In addition, the tendency of layered MXenes nanocrystals to restack reduces the interlayer distance and open surface area, thus limiting their further application as adsorbents. Molecular sieve membranes with sufficient and homogeneous nanochannels to break the permeation-selectivity equilibrium are ideal for efficient gas separation, and the resulting 2D materials offer new avenues for membrane development. However, for 2D layered membranes, the randomly stacked adjacent nanosheets usually form disordered interlayer nanochannels between them, hindering the efficient separation performance of the membranes. Hence, it remains challenging to prepare layered membranes with highly ordered nanochannel structures for fast and accurate molecular sieving.

4.3 Future prospects

Although the development of MXene-based membranes for gas separation is still in its infancy, it is clear that the results of the current study have shown the great promise for their application. Given the current state of research, "(1) the further exploration of the potential of MXenes may achieve better gas separation effects than other 2D materials or provide a wider range of application directions and (2) the gradual extension and application of proven methods for other materials to the study of MXenes, and an in-depth investigation of the combination of MXenes with other polymers or 2D materials to obtain the composite materials". With more research on these two aspects and taking full use of the advantages and properties of MXenes, the prepared separation membranes may have more obvious results. Currently, gas selectivity studies on MXene-based membranes are mainly based on the construction of the interlayer spacing of MXene nanosheets. In addition, the effects of the MXene nanosheet size, the interactions between gases and MXenes, and the applications in multi-material mixing systems have not been extensively studied, and thus all these aspects need to be further explored. Therefore, the research on MXenes has a very promising future.

Conflicts of interest

There are no conflicts to declare.

Acknowledgements

The project was funded by the National Natural Science Foundation of China (No. 51872245, 52103269), the Fok Ying-Tong Education Foundation of China (161044), the Natural Science Foundation of Gansu Province, China (20JR10RA106), the Scientific and Technical Innovation Project of Northwest Normal University (NWNU-LKQN2019-26), the innovation fund project of Gansu Higher Education Institutions (2020B-090). We also thank the Gansu International Scientific and Technological Cooperation Base of Water-Retention Chemical Functional Materials for financial support.

References

1 W. Cai, K. Li, H. Liao, H. Wang and L. Wu, *Nat. Clim. Change*, 2017, **7**, 257–262.
2 M. A. Malati, *Energy Convers. Manage.*, 1996, **37**, 1345–1350.
3 J. M. Mathias and R. B. Thomas, *Global Change Biol.*, 2018, **24**, 3938–3953.
4 M. A. Adams, T. N. Buckley, D. Binkley, M. Neumann and T. L. Turnbull, *Nat. Commun.*, 2021, **12**, 5194.
5 W. Cui, L. Cao, J. Liu, Z. Ren, B. Zhao and S. Dou, *Sci. Total Environ.*, 2020, **718**, 137234.

6 X. Jiang, S. Li and L. Shao, *Energy Environ. Sci.*, 2017, **10**, 1339–1344.
7 X. Duan, J. Xu, Z. Wei, J. Ma, S. Guo, S. Wang, H. Liu and S. Dou, *Adv. Mater.*, 2017, **29**, 1701784.
8 X. Tan, H. A. Tahini and S. C. Smith, *Curr. Opin. Electrochem.*, 2017, **4**, 118–123.
9 I. Sullivan, A. Goryachev, I. A. Digdaya, X. Li, H. A. Atwater, D. A. Vermaas and C. Xiang, *Nat. Catal.*, 2022, **5**, 75–76.
10 P. Szuromi, *Science*, 2020, **369**, 446.
11 Y. Du, Y. Wang and G. T. Rochelle, *Chem. Eng. J.*, 2017, **307**, 258–263.
12 H. Wang, Q. Tang and Z. Wu, *ACS Sustainable Chem. Eng.*, 2021, **9**, 8425–8434.
13 S. Roussanaly and R. Anantharaman, *Chem. Eng. J.*, 2017, **327**, 618–628.
14 F. Geyer, C. Schönecker, H. Butt and D. Vollmer, *Adv. Mater.*, 2017, **29**, 1603524.
15 J. Di, C. Zhu, M. Ji, M. Duan, R. Long, C. Yan, K. Gu, J. Xiong, Y. She, J. Xia, H. Li and Z. Liu, *Angew. Chem., Int. Ed.*, 2018, **57**, 14847–14851.
16 F. O. Ochedi, J. Yu, H. Yu, Y. Liu and A. Hussain, *Environ. Chem. Lett.*, 2020, **19**, 77–109.
17 W. Li, S. Choi, J. H. Drese, M. Hornbostel, G. Krishnan, P. M. Eisenberger and C. W. Jones, *Communications*, 2010, **3**, 899–903.
18 S. H. Goh, H. S. Lau and W. F. Yong, *Small*, 2022, **18**, 2107536.
19 Y. Han and W. S. W. Ho, *J. Membr. Sci.*, 2021, **628**, 119244.
20 G. Dong and Y. M. Lee, *J. Mater. Chem. A*, 2017, **5**, 13294–13319.
21 D. H. Seo, S. Pineda, Y. C. Woo, M. Xie, A. T. Murdock, E. Y. M. Ang, Y. Jiao, M. J. Park, S. I. Lim, M. Lawn, F. F. Borghi, Z. J. Han, S. Gray, G. Millar, A. Du, H. K. Shon, T. Y. Ng and K. K. Ostrikov, *Nat. Commun.*, 2018, **9**, 683.
22 Y. K. Ong, G. M. Shi, N. L. Le, Y. P. Tang, J. Zuo, S. P. Nunes and T.-S. Chung, *Prog. Polym. Sci.*, 2016, **57**, 1–31.
23 G. Liu and W. Jin, *J. Membr. Sci.*, 2021, **636**, 119557.
24 M. Wang, S. Zhou, S. Cao, Z. Wang, S. Liu, S. Wei, Y. Chen and X. Lu, *J. Mater. Chem. A*, 2020, **8**, 10519–10533.
25 H. Liu, P. Guo and G. Chen, *Sep. Purif. Technol.*, 2017, **189**, 66–73.
26 Y. Li, S. Wang, G. He, H. Wu, F. Pan and Z. Jiang, *Chem. Soc. Rev.*, 2015, **44**, 103–118.
27 K. Xie, Q. Fu, G. G. Qiao and P. A. Webley, *J. Membr. Sci.*, 2019, **572**, 38–60.
28 Z. Xu, Z. Fan, C. Shen, Q. Meng, G. Zhang and C. Gao, *Adv. Membr.*, 2022, **2**, 100027.
29 S. Wang, X. Li, H. Wu, Z. Tian, Q. Xin, G. He, D. Peng, S. Chen, Y. Yin, Z. Jiang and M. D. Guiver, *Energy Environ. Sci.*, 2016, **9**, 1863–1890.
30 X. Zou and G. Zhu, *Adv. Mater.*, 2018, **30**, 1700750.
31 B. M. Yoo, J. E. Shin, H. D. Lee and H. B. Park, *Curr. Opin. Chem. Eng.*, 2017, **16**, 39–47.
32 Z. Tian, S. M. Mahurin, S. Dai and D. E. Jiang, *Nano Lett.*, 2017, **17**, 1802–1807.
33 M. Asghari, S. Saadatmandi and M. Afsari, *ChemBioEng Rev.*, 2021, **8**, 490–516.
34 S. Ma, Z. Tang, Y. Fan, J. Zhao, X. Meng, N. Yang, S. Zhuo and S. Liu, *Carbon*, 2019, **152**, 144–150.
35 Y. Wang, B. Gao, Q. Yue and Z. Wang, *J. Mater. Chem. A*, 2020, **8**, 19133–19155.
36 Y. Wang, G. Tan, M. Dang, S. Dong, Y. Liu, T. Liu, H. Ren, A. Xia and L. Lv, *J. Alloys Compd.*, 2022, **908**, 164507.
37 Z. Niu, W. Luo, P. Mu and J. Li, *Sep. Purif. Technol.*, 2022, **297**, 121513.
38 K. Huang, L. Liang, S. Chai, U. Tumuluri, M. Li, Z. Wu, B. G. Sumpter and S. Dai, *J. Mater. Chem. A*, 2017, **5**, 16241–16248.
39 Y. Li, L. Liu, H. Yu, Y. Zhao, J. Dai, Y. Zhong, Z. Pan and H. Yu, *Sci. Total Environ.*, 2022, **811**, 151384.
40 X. Wan, T. Wan, C. Cao, C. Tang, Y. Xue, Y. Yan, Z. Li, Z. Ye and X. Peng, *Chem. Eng. J.*, 2021, **423**, 130309.
41 J. Fonseca, T. Gong, L. Jiao and H.-L. Jiang, *J. Mater. Chem. A*, 2021, **9**, 10562–10611.
42 B. Li, H. M. Wen, Y. Yu, Y. Cui, W. Zhou, B. Chen and G. Qian, *Mater. Today Nano*, 2018, **2**, 21–49.
43 C. Kong, H. Du, L. Chen and B. Chen, *Energy Environ. Sci.*, 2017, **10**, 1812–1819.
44 Y. Zeng, R. Zou and Y. Zhao, *Adv. Mater.*, 2016, **28**, 2855–2873.
45 R. Luo, Y. Yang, K. Chen, X. Liu, M. Chen, W. Xu, B. Liu, H. Ji and Y. Fang, *J. Mater. Chem. A*, 2021, **9**, 20941–20956.
46 A. A. Wani, A. M. Khan, Y. K. Manea, M. Shahadat, S. Z. Ahammad and S. W. Ali, *J. Cleaner Prod.*, 2020, **273**, 122980.
47 X. Liu, T. Ma, N. Pinna and J. Zhang, *Adv. Funct. Mater.*, 2017, **27**, 1702168.
48 G. Liu, W. Jin and N. Xu, *Angew. Chem., Int. Ed.*, 2016, **55**, 13384–13397.
49 H. Zhu and D. Liu, *J. Mater. Chem. A*, 2019, **7**, 21004–21035.
50 B. K. Voon, H. Shen Lau, C. Z. Liang and W. F. Yong, *Sep. Purif. Technol.*, 2022, **296**, 121354.
51 S. Bi, C. Lu, W. Zhang, F. Qiu and F. Zhang, *J. Energy Chem.*, 2018, **27**, 99–116.
52 Y. Ge, Z. Shi, C. Tan, Y. Chen, H. Cheng, Q. He and H. Zhang, *Chem*, 2020, **6**, 1237–1253.
53 F. Guo, D. Li, R. Ding, J. Gao, X. Ruan, X. Jiang, G. He and W. Xiao, *Sep. Purif. Technol.*, 2022, **280**, 119803.
54 P. Lu, Y. Liu, T. Zhou, Q. Wang and Y. Li, *J. Membr. Sci.*, 2018, **567**, 89–103.
55 M. Liu, P. A. Gurr, Q. Fu, P. A. Webley and G. G. Qiao, *J. Mater. Chem. A*, 2018, **6**, 23169–23196.
56 B. Anasori, M. R. Lukatskaya and Y. Gogotsi, *Nat. Rev. Mater.*, 2017, **2**, 16098.
57 Q. Zhao, Q. Zhu, J. Miao, P. Zhang and B. Xu, *Nanoscale*, 2019, **11**, 8442–8448.
58 T. Liu, C. Zhang and X. Li, *Adv. Opt. Mater.*, 2022, **10**, 2201153.

59 Y. Sun, X. Meng, Y. Dall'Agnese, C. Dall'Agnese, S. Duan, Y. Gao, G. Chen and X. F. Wang, *Nanomicro Lett.*, 2019, **11**, 79.
60 A. Rafieerad, W. Yan, G. L. Sequiera, N. Sareen, E. Abu-El-Rub, M. Moudgil and S. Dhingra, *Adv. Healthcare Mater.*, 2019, **8**, 1900569.
61 H. Huang, C. Dong, W. Feng, Y. Wang, B. Huang and Y. Chen, *Adv. Drug Delivery Rev.*, 2022, **184**, 114178.
62 T. Rasheed, *J. Mater. Chem. A*, 2022, **10**, 4558–4584.
63 J. Xu, X. Zhong, X. Wu, Y. Wang and S. Feng, *J. Energy Chem.*, 2022, **71**, 129–140.
64 M. Malaki, A. Maleki and R. S. Varma, *J. Mater. Chem. A*, 2019, **7**, 10843–10857.
65 M. Dadashi Firouzjaei, M. Karimiziarani, H. Moradkhani, M. Elliott and B. Anasori, *Mater. Today Adv.*, 2022, **13**, 100202.
66 P. Serles, M. Hamidinejad, P. G. Demingos, L. Ma, N. Barri, H. Taylor, C. V. Singh, C. B. Park and T. Filleter, *Nano Lett.*, 2022, **22**, 3356–3363.
67 D. B. Velusamy, J. K. El-Demellawi, A. M. El-Zohry, A. Giugni, S. Lopatin, M. N. Hedhili, A. E. Mansour, E. D. Fabrizio, O. F. Mohammed and H. N. Alshareef, *Adv. Mater.*, 2019, **31**, 1807658.
68 L. Yin, Y. Li, X. Yao, Y. Wang, L. Jia, Q. Liu, J. Li, Y. Li and D. He, *Nanomicro Lett.*, 2021, **13**, 78.
69 Y. Wang, T. Guo, Z. Tian, K. Bibi, Y. Z. Zhang and H. N. Alshareef, *Adv. Mater.*, 2022, **34**, 2108560.
70 Y. Cheng, W. Zhu, X. Lu and C. Wang, *Nano Energy*, 2022, **98**, 107229.
71 M. Q. Zhao, X. Xie, C. E. Ren, T. Makaryan, B. Anasori, G. Wang and Y. Gogotsi, *Adv. Mater.*, 2017, **29**, 1702410.
72 S. J. Kim, J. Choi, K. Maleski, K. Hantanasirisakul, H. T. Jung, Y. Gogotsi and C. W. Ahn, *ACS Appl. Mater. Interfaces*, 2019, **11**, 32320–32327.
73 J. Shen, G. Liu, Y. Ji, Q. Liu, L. Cheng, K. Guan, M. Zhang, G. Liu, J. Xiong, J. Yang and W. Jin, *Adv. Funct. Mater.*, 2018, **28**, 1801511.
74 Y. Xu, W. Zhang, Z. Li, L. Shen, R. Li, M. Zhang, Y. Jiao, H. Lin and C. Y. Tang, *J. Mater. Chem. A*, 2022, **10**, 16430–16438.
75 L. Ding, Y. Wei, L. Li, T. Zhang, H. Wang, J. Xue, L.-X. Ding, S. Wang, J. Caro and Y. Gogotsi, *Nat. Commun.*, 2018, **9**, 155.
76 C. Sun and B. Bai, *Sci. Bull.*, 2017, **62**, 554–562.
77 H. E. Karahan, K. Goh, C. J. Zhang, E. Yang, C. Yildirim, C. Y. Chuah, M. G. Ahunbay, J. Lee, S. B. Tantekin-Ersolmaz, Y. Chen and T. H. Bae, *Adv. Mater.*, 2020, **32**, 1906697.
78 Y. Huang, Q. Lu, D. Wu, Y. Jiang, Z. Liu, B. Chen, M. Zhu and O. G. Schmidt, *Carbon Energy*, 2022, **4**, 598–620.
79 J. Li, X. Li and B. Van der Bruggen, *Environ. Sci.: Nano*, 2020, **7**, 1289–1304.
80 Y.-J. Wan, K. Rajavel, X.-M. Li, X.-Y. Wang, S.-Y. Liao, Z.-Q. Lin, P.-L. Zhu, R. Sun and C.-P. Wong, *Chem. Eng. J.*, 2021, **408**, 127303.
81 K. Li, S. Zhang, Y. Li, J. Fan and K. Lv, *Chin. J. Catal.*, 2021, **42**, 3–14.
82 H. Kim, Z. Wang and H. N. Alshareef, *Nano Energy*, 2019, **60**, 179–197.
83 D. Johnson, Z. Qiao, E. Uwadiunor and A. Djire, *Small*, 2022, **18**, 2106129.
84 S. Wang, F. Wang, Y. Jin, X. Meng, B. Meng, N. Yang, J. Sunarso and S. Liu, *J. Membr. Sci.*, 2021, **638**, 119697.
85 A. A. Shamsabadi, A. P. Isfahani, S. K. Salestan, A. Rahimpour, B. Ghalei, E. Sivaniah and M. Soroush, *ACS Appl. Mater. Interfaces*, 2020, **12**, 3984–3992.
86 G. Liu, J. Shen, Q. Liu, G. Liu, J. Xiong, J. Yang and W. Jin, *J. Membr. Sci.*, 2018, **548**, 548–558.
87 R. Malik, *Joule*, 2018, **2**, 591–593.
88 G. Liu, J. Shen, Y. Ji, Q. Liu, G. Liu, J. Yang and W. Jin, *J. Mater. Chem. A*, 2019, **7**, 12095–12104.
89 M. Naguib, V. N. Mochalin, M. W. Barsoum and Y. Gogotsi, *Adv. Mater.*, 2014, **26**, 992–1005.
90 M. Alhabeb, K. Maleski, B. Anasori, P. Lelyukh, L. Clark, S. Sin and Y. Gogotsi, *Chem. Mater.*, 2017, **29**, 7633–7644.
91 M. Naguib, J. Come, B. Dyatkin, V. Presser, P.-L. Taberna, P. Simon, M. W. Barsoum and Y. Gogotsi, *Electrochem. Commun.*, 2012, **16**, 61–64.
92 K. V. Mahesh, S. Balanand, R. Raimond, A. Peer Mohamed and S. Ananthakumar, *Mater. Des.*, 2014, **63**, 360–367.
93 H. Lin, K. Gong, P. Hykys, D. Chen, W. Ying, Z. Sofer, Y. Yan, Z. Li and X. Peng, *Chem. Eng. J.*, 2021, **405**, 126961.
94 O. M. M. Naguib, J. Carle, V. Presser, J. Lu, L. Hultman, Y. Gogotsi and M. W. Barsoum, *ACS Nano*, 2012, **6**, 1322–1331.
95 M. Han, X. Yin, H. Wu, Z. Hou, C. Song, X. Li, L. Zhang and L. Cheng, *ACS Appl. Mater. Interfaces*, 2016, **8**, 21011–21019.
96 F. Kong, X. He, Q. Liu, X. Qi, Y. Zheng, R. Wang and Y. Bai, *Electrochim. Acta*, 2018, **265**, 140–150.
97 Y. Fang, X. Yang, T. Chen, G. Xu, M. Liu, J. Liu and Y. Xu, *Sens. Actuators, B*, 2018, **263**, 400–407.
98 Y. Wei, P. Zhang, R. A. Soomro, Q. Zhu and B. Xu, *Adv. Mater.*, 2021, **33**, 2103148.
99 L.-Y. Xiu, Z.-Y. Wang and J.-S. Qiu, *Rare Met.*, 2020, **39**, 1237–1238.
100 Y. Gogotsi and B. Anasori, *ACS Nano*, 2019, **13**, 8491–8494.
101 B. Xu and Y. Gogotsi, *Chin. Chem. Lett.*, 2020, **31**, 919–921.
102 Z. Sun, D. Music, R. Ahuja, S. Li and J. M. Schneider, *Phys. Rev. B: Condens. Matter Mater. Phys.*, 2004, **70**, 092102.
103 M. R. Lukatskaya, O. Mashtalir, C. E. Ren, Y. Dall'Agnese, P. Rozier, P. L. Taberna, M. Naguib, P. Simon, M. W. Barsoum and Y. Gogotsi, *Science*, 2013, **341**, 1502–1505.
104 O. Mashtalir, M. Naguib, B. Dyatkin, Y. Gogotsi and M. W. Barsoum, *Mater. Chem. Phys.*, 2013, **139**, 147–152.
105 J. Halim, M. R. Lukatskaya, K. M. Cook, J. Lu, C. R. Smith, L. A. Naslund, S. J. May, L. Hultman, Y. Gogotsi, P. Eklund and M. W. Barsoum, *Chem. Mater.*, 2014, **26**, 2374–2381.
106 C. Peng, P. Wei, X. Chen, Y. Zhang, F. Zhu, Y. Cao, H. Wang, H. Yu and F. Peng, *Ceram. Int.*, 2018, **44**, 18886–18893.

107 A. Feng, Y. Yu, Y. Wang, F. Jiang, Y. Yu, L. Mi and L. Song, *Mater. Des.*, 2017, **114**, 161–166.
108 Y. Xia, T. S. Mathis, M. Q. Zhao, B. Anasori, A. Dang, Z. Zhou, H. Cho, Y. Gogotsi and S. Yang, *Nature*, 2018, **557**, 409–412.
109 M. R. Lukatskaya, S. Kota, Z. Lin, M.-Q. Zhao, N. Shpigel, M. D. Levi, J. Halim, P.-L. Taberna, M. W. Barsoum, P. Simon and Y. Gogotsi, *Nat. Energy*, 2017, **2**, 17105.
110 W. Tian, A. VahidMohammadi, Z. Wang, L. Ouyang, M. Beidaghi and M. M. Hamedi, *Nat. Commun.*, 2019, **10**, 2558.
111 S. J. Kim, H. J. Koh, C. E. Ren, O. Kwon, K. Maleski, S. Y. Cho, B. Anasori, C. K. Kim, Y. K. Choi, J. Kim, Y. Gogotsi and H. T. Jung, *ACS Nano*, 2018, **12**, 986–993.
112 J. Choi, Y. J. Kim, S. Y. Cho, K. Park, H. Kang, S. J. Kim and H. T. Jung, *Adv. Funct. Mater.*, 2020, **30**, 2003998.
113 M. Naguib, M. Kurtoglu, V. Presser, J. Lu, J. Niu, M. Heon, L. Hultman, Y. Gogotsi and M. W. Barsoum, *Adv. Mater.*, 2011, **23**, 4248–4253.
114 P. Srivastava, A. Mishra, H. Mizuseki, K. R. Lee and A. K. Singh, *ACS Appl. Mater. Interfaces*, 2016, **8**, 24256–24264.
115 C. G. Pope, *J. Chem. Educ.*, 1997, **74**, 129.
116 Y. Ying, Y. Liu, X. Wang, Y. Mao, W. Cao, P. Hu and X. Peng, *ACS Appl. Mater. Interfaces*, 2015, **7**, 1795–1803.
117 J. Zhou, X. Zha, X. Zhou, F. Chen, G. Gao, S. Wang, C. Shen, T. Chen, C. Zhi, P. Eklund, S. Du, J. Xue, W. Shi, Z. Chai and Q. Huang, *ACS Nano*, 2017, **11**, 3841–3850.
118 Q. Tang, Z. Zhou and P. Shen, *J. Am. Chem. Soc.*, 2012, **134**, 16909–16916.
119 F. Liu, A. Zhou, J. Chen, J. Jia, W. Zhou, L. Wang and Q. Hu, *Appl. Surf. Sci.*, 2017, **416**, 781–789.
120 M. Ghidiu, M. R. Lukatskaya, M. Q. Zhao, Y. Gogotsi and M. W. Barsoum, *Nature*, 2014, **516**, 78–81.
121 X. Wang, C. Garnero, G. Rochard, D. Magne, S. Morisset, S. Hurand, P. Chartier, J. Rousseau, T. Cabioc'h, C. Coutanceau, V. Mauchamp and S. Célérier, *J. Mater. Chem. A*, 2017, **5**, 22012–22023.
122 Z. Lin, D. Barbara, P.-L. Taberna, K. L. Van Aken, B. Anasori, Y. Gogotsi and P. Simon, *J. Power Sources*, 2016, **326**, 575–579.
123 Y. Zhu, J. Liu, T. Guo, J. J. Wang, X. Tang and V. Nicolosi, *ACS Nano*, 2021, **15**, 1465–1474.
124 C. Zhou, X. Zhao, Y. Xiong, Y. Tang, X. Ma, Q. Tao, C. Sun and W. Xu, *Eur. Polym. J.*, 2022, **167**, 111063.
125 Y.-J. Kim, S. J. Kim, D. Seo, Y. Chae, M. Anayee, Y. Lee, Y. Gogotsi, C. W. Ahn and H.-T. Jung, *Chem. Mater.*, 2021, **33**, 6346–6355.
126 A. Feng, Y. Yu, L. Mi, Y. Yu and L. Song, *Ionics*, 2018, **25**, 727–735.
127 A. Feng, Y. Yu, F. Jiang, Y. Wang, L. Mi, Y. Yu and L. Song, *Ceram. Int.*, 2017, **43**, 6322–6328.
128 J. Wu, Y. Wang, Y. Zhang, H. Meng, Y. Xu, Y. Han, Z. Wang, Y. Dong and X. Zhang, *J. Energy Chem.*, 2020, **47**, 203–209.
129 C. B. Cockreham, V. G. Goncharov, E. Hammond-Pereira, M. E. Reece, A. C. Strzelecki, W. Xu, S. R. Saunders, H. Xu, X. Guo and D. Wu, *ACS Appl. Mater. Interfaces*, 2022, **14**, 41542–41554.
130 W. Sun, S. A. Shah, Y. Chen, Z. Tan, H. Gao, T. Habib, M. Radovic and M. J. Green, *J. Mater. Chem. A*, 2017, **5**, 21663–21668.
131 R. Luo, R. Li, C. Jiang, R. Qi, M. Liu, C. Luo, H. Lin, R. Huang and H. Peng, *Int. J. Hydrogen Energy*, 2021, **46**, 32536–32545.
132 S. Yang, P. Zhang, F. Wang, A. G. Ricciardulli, M. R. Lohe, P. W. M. Blom and X. Feng, *Angew. Chem., Int. Ed.*, 2018, **57**, 15491–15495.
133 H. Lin, Z. Shi, S. He, X. Yu, S. Wang, Q. Gao and Y. Tang, *Chem. Sci.*, 2016, **7**, 3399–3405.
134 E. S. Sim and Y.-C. Chung, *Appl. Surf. Sci.*, 2018, **435**, 210–215.
135 K. Huang, Z. Li, J. Lin, G. Han and P. Huang, *Chem. Soc. Rev.*, 2018, **47**, 5109–5124.
136 M. Khazaei, M. Arai, T. Sasaki, C.-Y. Chung, N. S. Venkataramanan, M. Estili, Y. Sakka and Y. Kawazoe, *Adv. Funct. Mater.*, 2013, **23**, 2185–2192.
137 T. Hu, Z. Li, M. Hu, J. Wang, Q. Hu, Q. Li and X. Wang, *J. Phys. Chem. C*, 2017, **121**, 19254–19261.
138 Z. Fu, N. Wang, D. Legut, C. Si, Q. Zhang, S. Du, T. C. Germann, J. S. Francisco and R. Zhang, *Chem. Rev.*, 2019, **119**, 11980–12031.
139 C. H. Kwak, C. Lim, S. Kim and Y.-S. Lee, *J. Ind. Eng. Chem.*, 2022, **116**, 21–31.
140 J. Y. S. Lin, *Science*, 2016, **353**, 121–122.
141 X. Zhang, Q. Huang, F. Deng, H. Huang, Q. Wan, M. Liu and Y. Wei, *Appl. Mater. Today*, 2017, **7**, 222–238.
142 X. Zhang, Q. Huang, M. Liu, J. Tian, G. Zeng, Z. Li, K. Wang, Q. Zhang, Q. Wan, F. Deng and Y. Wei, *Appl. Surf. Sci.*, 2015, **343**, 19–27.
143 Q. Huang, M. Liu, L. Mao, D. Xu, G. Zeng, H. Huang, R. Jiang, F. Deng, X. Zhang and Y. Wei, *J. Colloid Interface Sci.*, 2017, **499**, 170–179.
144 H. Shen, L. Zhang, M. Liu and Z. Zhang, *Theranostics*, 2012, **2**, 283–294.
145 C. Tan, X. Huang and H. Zhang, *Mater. Today*, 2013, **16**, 29–36.
146 M. Zhang, Y. Li, Z. Su and G. Wei, *Polym. Chem.*, 2015, **6**, 6107–6124.
147 X. Wang, R. Yin, L. Zeng and M. Zhu, *Environ. Pollut.*, 2019, **253**, 100–110.
148 S. Kim, C. M. Park, M. Jang, A. Son, N. Her, M. Yu, S. Snyder, D. H. Kim and Y. Yoon, *Chemosphere*, 2018, **212**, 1104–1124.
149 X. Liu, R. Ma, X. Wang, Y. Ma, Y. Yang, L. Zhuang, S. Zhang, R. Jehan, J. Chen and X. Wang, *Environ. Pollut.*, 2019, **252**, 62–73.
150 M. Khazaei, M. Arai, T. Sasaki, A. Ranjbar, Y. Liang and S. Yunoki, *Phys. Rev. B: Condens. Matter Mater. Phys.*, 2015, **92**, 075411.

151 M. Ye, X. Wang, E. Liu, J. Ye and D. Wang, *ChemSusChem*, 2018, **11**, 1606–1611.
152 Z. Wei, Z. Peigen, T. Wubian, Q. Xia, Z. Yamei and S. ZhengMing, *Mater. Chem. Phys.*, 2018, **206**, 270–276.
153 M. Peng, M. Dong, W. Wei, H. Xu, C. Liu and C. Shen, *Carbon*, 2021, **179**, 400–407.
154 R. Luo, W. Zhang, X. Hu, Y. Liang, J. Fu, M. Liu, F. Deng, Q.-Y. Cao, X. Zhang and Y. Wei, *Appl. Surf. Sci.*, 2022, **602**, 154197.
155 H. Riazi, M. Anayee, K. Hantanasirisakul, A. A. Shamsabadi, B. Anasori, Y. Gogotsi and M. Soroush, *Adv. Mater. Interfaces*, 2020, **7**, 1902008.
156 D. Gan, Q. Huang, J. Dou, H. Huang, J. Chen, M. Liu, Y. Wen, Z. Yang, X. Zhang and Y. Wei, *Appl. Surf. Sci.*, 2020, **504**, 144603.
157 M. Elimelech and W. A. Phillip, *Science*, 2011, **333**, 712–717.
158 C. R. Holkar, A. J. Jadhav, D. V. Pinjari, N. M. Mahamuni and A. B. Pandit, *J. Environ. Manage.*, 2016, **182**, 351–366.
159 J. Luo and Y. Wan, *J. Membr. Sci.*, 2011, **372**, 145–153.
160 T. Tavangar, M. Karimi, M. Rezakazemi, K. R. Reddy and T. M. Aminabhavi, *Chem. Eng. J.*, 2020, **385**, 123787.
161 S. Yu, C. Gao, H. Su and M. Liu, *Desalination*, 2001, **140**, 97–100.
162 Y. Lei, Y. Cui, Q. Huang, J. Dou, D. Gan, F. Deng, M. Liu, X. Li, X. Zhang and Y. Wei, *Ceram. Int.*, 2019, **45**, 17653–17661.
163 H. Wang, Z. He, Q. Yang, G. Zeng, Z. Yang and S. Pu, *J. Environ. Chem. Eng.*, 2022, **10**, 108365.
164 W. L. Xu, C. Fang, F. Zhou, Z. Song, Q. Liu, R. Qiao and M. Yu, *Nano Lett.*, 2017, **17**, 2928–2933.
165 J. Shen, G. Liu, K. Huang, Z. Chu, W. Jin and N. Xu, *ACS Nano*, 2016, **10**, 3398–3409.
166 X. Wang, C. Chi, K. Zhang, Y. Qian, K. M. Gupta, Z. Kang, J. Jiang and D. Zhao, *Nat. Commun.*, 2017, **8**, 14460.
167 I. S. Sadilov, D. I. Petukhov and A. A. Eliseev, *Sep. Purif. Technol.*, 2019, **221**, 74–82.
168 M. Rezakazemi, A. Arabi Shamsabadi, H. Lin, P. Luis, S. Ramakrishna and T. M. Aminabhavi, *Renewable Sustainable Energy Rev.*, 2021, **143**, 110878.
169 F. Shi, J. Sun, J. Wang, M. Liu, Z. Yan, B. Zhu, Y. Li and X. Cao, *J. Membr. Sci.*, 2021, **620**, 118850.
170 L. Li, T. Zhang, Y. Duan, Y. Wei, C. Dong, L. Ding, Z. Qiao and H. Wang, *J. Mater. Chem. A*, 2018, **6**, 11734–11742.
171 Y. Jia, F. Shi, H. Li, Z. Yan, J. Xu, J. Gao, X. Wu, Y. Li, J. Wang and B. Zhang, *ACS Nano*, 2022, **16**, 14379–14389.
172 J. Grünauer, V. Filiz, S. Shishatskiy, C. Abetz and V. Abetz, *J. Membr. Sci.*, 2016, **518**, 178–191.
173 X. Hong, Z. Lu, Y. Zhao, L. Lyu, L. Ding, Y. Wei and H. Wang, *J. Membr. Sci.*, 2022, **642**, 119982.
174 Z. Wang, Q. Tu, S. Zheng, J. J. Urban, S. Li and B. Mi, *Nano Lett.*, 2017, **17**, 7289–7298.
175 H. Zhou, Y. Wang, F. Wang, H. Deng, Y. Song, C. Li and Z. Ling, *Chin. Chem. Lett.*, 2020, **31**, 1665–1669.
176 A. P. Isfahani, A. Arabi Shamsabadi and M. Soroush, *Ind. Eng. Chem. Res.*, 2022, DOI: **10.1021/acs.iecr.2c02042**.
177 A. Al-Temimy, B. Anasori, K. A. Mazzio, F. Kronast, M. Seredych, N. Kurra, M.-A. Mawass, S. Raoux, Y. Gogotsi and T. Petit, *J. Phys. Chem. C*, 2020, **124**, 5079–5086.
178 J. Li, X. Yuan, C. Lin, Y. Yang, L. Xu, X. Du, J. Xie, J. Lin and J. Sun, *Adv. Energy Mater.*, 2017, **7**, 1602725.
179 M. Ghidiu, J. Halim, S. Kota, D. Bish, Y. Gogotsi and M. W. Barsoum, *Chem. Mater.*, 2016, **28**, 3507–3514.
180 H. J. Koh, S. J. Kim, K. Maleski, S. Y. Cho, Y. J. Kim, C. W. Ahn, Y. Gogotsi and H. T. Jung, *ACS Sens.*, 2019, **4**, 1365–1372.
181 Q. Gao, J. Come, M. Naguib, S. Jesse, Y. Gogotsi and N. Balke, *Faraday Discuss.*, 2017, **199**, 393–403.
182 O. Mashtalir, M. R. Lukatskaya, A. I. Kolesnikov, E. Raymundo-Pinero, M. Naguib, M. W. Barsoum and Y. Gogotsi, *Nanoscale*, 2016, **8**, 9128–9133.
183 H. Pazniak, M. Benchakar, T. Bilyk, A. Liedl, Y. Busby, C. Noel, P. Chartier, S. Hurand, M. Marteau, L. Houssiau, R. Larciprete, P. Lacovig, D. Lizzit, E. Tosi, S. Lizzit, J. Pacaud, S. Celerier, V. Mauchamp and M. L. David, *ACS Nano*, 2021, **15**, 4245–4255.
184 L. Ding, Y. Wei, Y. Wang, H. Chen, J. Caro and H. Wang, *Angew. Chem., Int. Ed.*, 2017, **56**, 1825–1829.
185 Y. Fan, J. Li, S. Wang, X. Meng, Y. Jin, N. Yang, B. Meng, J. Li and S. Liu, *Front. Chem. Sci. Eng.*, 2020, **15**, 882–891.
186 Z. Zhao, L. Ding, R. Hinterding, A. Mundstock, C. Belke, R. J. Haug, H. Wang and A. Feldhoff, *J. Membr. Sci.*, 2022, **652**, 120432.
187 K. Qu, L. Dai, Y. Xia, Y. Wang, D. Zhang, Y. Wu, Z. Yao, K. Huang, X. Guo and Z. Xu, *J. Membr. Sci.*, 2021, **638**, 119669.